Weierstraß-Institut

für Angewandte Analysis und Stochastik

Leibniz-Institut im Forschungsverbund Berlin e. V.

Preprint ISSN 2198-5855

On really locking-free mixed finite element methods for the transient incompressible Stokes equations

Naveed Ahmed, Alexander Linke, Christian Merdon

submitted: January 20, 2017

Weierstrass Institute
Mohrenstr. 39
10117 Berlin
Germany
email: naveed.ahmed@wias-berlin.de
alexander.linke@wias-berlin.de
christian.merdon@wias-berlin.de

No. 2368

Berlin 2017

2010 *Mathematics Subject Classification.* 65M12, 665M30, 65M15, 76D07, 76M10.

Key words and phrases. transient incompressible Stokes equations, mixed finite element methods, locking phenomenon, pressure-robustness, a priori error analysis.

Edited by
Weierstraß-Institut für Angewandte Analysis und Stochastik (WIAS)
Leibniz-Institut im Forschungsverbund Berlin e. V.
Mohrenstraße 39
10117 Berlin
Germany

Fax: +49 30 20372-303
E-Mail: preprint@wias-berlin.de
World Wide Web: http://www.wias-berlin.de/

Abstract

Inf-sup stable mixed methods for the steady incompressible Stokes equations that relax the divergence constraint are often claimed to deliver locking-free discretizations. However, this relaxation leads to a pressure-dependent contribution in the velocity error, which is proportional to the inverse of the viscosity, thus giving rise to a (different) locking phenomenon. However, a recently proposed modification of the right hand side alone leads to a discretization that is really locking-free, i.e., its velocity error converges with optimal order and is independent of the pressure and the smallness of the viscosity. In this contribution, we extend this approach to the transient incompressible Stokes equations, where besides the right hand side also the velocity time derivative requires an improved space discretization. Semi-discrete and fully-discrete a-priori velocity and pressure error estimates are derived, which show beautiful robustness properties. Two numerical examples illustrate the superior accuracy of pressure-robust space discretizations in the case of small viscosities.

1 Introduction

In the seventies [17, 11, 22], numerical analysts found out how to construct finite element discretizations for the steady incompressible Stokes equations, which converge with optimal order. The challenge consisted in the phenomenon of Poisson locking — well-known from linear elasticity theory [5] —, which is related to the discretization of the divergence constraint. The breakthrough observation was that slightly relaxing the divergence constraint enables an easier construction of optimal order algorithms. However, numerical analysts at that time did not investigate in depth that relaxing the divergence constraint is dangerous and leads to another locking phenomenon [26] — sometimes (rather imprecisely) called poor mass conservation [29, 21] —, mirrored by a pressure-dependent contribution in the velocity error that is proportional to the inverse of the viscosity [26, 32, 15, 36, 9, 18, 35]. In short, classical mixed methods for the incompressible Stokes equations like the nonconforming Crouzeix–Raviart element, the mini element or the Taylor–Hood element have replaced Poisson locking by another locking phenomenon [26, 34, 21, 7].

However, a closer look on the issue has recently revealed that relaxing the divergence constraint is only dangerous in the velocity test functions and not in the velocity trial functions [32, 26]. Moreover, it has been shown that classical mixed methods work well for divergence-free forces [32, 26], and that 'poor mass conservation' is in fact excited by an inaccurate treatment of large irrotational forces in the discrete momentum balance [26, 33, 32]. Such velocity errors may appear, since relaxing the divergence constraint in discrete velocity test functions induces a discrete L^2 scalar product for vector fields, where discretely divergence-free functions are only approximately orthogonal to irrotational vector fields [32, 26]. This observation has led to novel pressure-robust mixed methods for the steady incompressible Stokes equations, which have the same stiffness matrix as classical mixed methods, but discretize the right hand side forcing differently [32, 36, 30, 9, 18, 35]. Thus, improved scalar products for L^2 vector fields with better orthogonality properties lead to really locking-free mixed methods, where the velocity error does not depend on the pressure and not on the inverse of the viscosity, either.

In this sense, classical divergence-free mixed methods like the Scott–Vogelius element [42, 4, 41] and novel divergence-free mixed methods [31, 20, 16, 23, 14, 19] — whose spaces of discretely divergence-free vector fields are really divergence-free in the sense of $H(\mathrm{div};\Omega)$ — build an (important) subclass

of all possible pressure-robust methods. Since their discretely divergence-free velocity test functions are really divergence-free, there is no need for an improved L^2 scalar product for vector fields. But note, please, that classical mixed methods have just been invented, in order to replace *divergence-free* mixed methods [11, 22] assuming these schemes would be inefficient in practical computations, e.g., due to the high order of their approximation spaces [43, 41], the (additional) necessary barycentric refinement [42], or the use of rational bubble functions [23].

In this contribution, we now extend previous work on pressure-robust mixed methods for the *steady* incompressible Stokes equations to the *time-dependent* case. The *transient incompressible Stokes equations* $\mathbf{u}_t - \nu\Delta\mathbf{u} + \nabla p = \mathbf{f}$, $\nabla \cdot \mathbf{u} = 0$, equipped with certain initial and boundary conditions, are significantly more difficult to handle than the steady ones. Especially, in stabilized (equal-order) mixed methods there is some ongoing debate on how to choose an appropriate discrete initial value for the time evolution [13, 12, 2], how to overcome restrictions on a minimal time step [8, 13, 12, 2], how to choose the necessary (pressure-)stabilization parameter [28, 12, 6] and how to mitigate *poor mass conservation* (see the discussion above) by grad-div stabilization [28, 38, 15, 25, 39, 1]. Further, in stabilized mixed methods strange dependencies of the velocity and pressure errors on the initial pressure $(p - p_h)(0)$ are reported [28].

Amazingly, a numerical error analysis for *pressure-robust* (or *divergence-free*) mixed methods for the transient incompressible Stokes equations has never been presented before — to the best of the knowledge of the authors, though recently in [37] an attempt was made to analyze a pressure-robust discretization for the transient incompressible *Navier–Stokes* equations. But due to a focus on *some difficulties* involved by the nonlinear convection term the authors did not look at potential advantages of pressure-robustness for the *transient incompressible Stokes subsystem*.

Therefore, we emphasize in this contribution the beautiful robustness properties of *pressure-robust* mixed methods for the *transient incompressible Stokes equations*. All the ambiguities concerning the discrete initial value have gone, and neither time step restrictions nor stabilization parameters are needed. For example, in the limit case $\nu = 0$, a time-continuous, space-discrete pressure-robust mixed discretization will deliver the L^2 best approximation in every time point in some space of divergence-free vector fields. On the contrary, a classical mixed method that relaxes the divergence constraint can develop in this situation arbitrarily large velocity errors in long-time computations. Our analysis reveals that in the time-dependent case *pressure-robust* mixed methods need not only to improve the standard right hand side (space) discretization of $\mathbf{f}$ (as in the steady problem), but also the space discretization of the time derivative $\mathbf{u}_t$. Indeed, the novel non-standard space discretization of $\mathbf{u}_t$ makes it possible that for $\nu = 0$ the semi-discrete scheme delivers the L^2 best approximation in every time point. Moreover, this improvement also pays off in time-dependent potential flows as recently demonstrated in [34]. In fact, for time-dependent potential flows a pressure-robust (space) discretization may allow for drastically larger time steps without compromising the numerical accuracy. Briefly, the main highlights of this contribution are:

1 a *pressure-robust* space discretization of the transient incompressible Stokes equations requires to improve the two L^2 scalar products $(\mathbf{u}_{h,t}, \mathbf{v}_h)$ and $(\mathbf{f}, \mathbf{v}_h)$;

2 several a priori error estimates are presented that involve *discrete Helmholtz projectors* [34] as a new analytical tool;

3 numerical examples using classical and pressure-robust variants of the P_2^{bub}-P_1^{disc} and the Bernardi–Raugel elements are presented that illustrate the theory.

The rest of the paper is structured as follows. Section 2 introduces the model problem and some notation. Section 3 recalls classical inf-sup stable mixed finite element methods and their modified pressure-robust

siblings, including a novel (space) discretization of the time derivative. Section 4 concerns the limit case for $\nu = 0$ and some L^2 best approximation results. Section 5 then also discretizes in time with the help of the θ-schemes with $\theta = 0.5$ or $\theta = 1$. In this section, also stability results and some a-priori error estimates for the fully discrete classical and pressure-robust schemes are derived. Eventually, Section 6 studies some numerical examples to demonstrate the improved numerical accuracy of pressure-robust mixed methods in certain benchmark problems.

2 Model problem and preliminaries

Let Ω be a domain in $\mathbb{R}^d$ ($d = 2$ or 3), with a polyhedral boundary. For $T > 0$, consider the problem: for $\mathbf{u} : \Omega \times (0,T) \to \mathbb{R}^d$ and $p : \Omega \times (0,T) \to \mathbb{R}$, find the solution of the following time-dependent Stokes equations:

$$\left\{\begin{array}{rll} \mathbf{u}_t - \nu\Delta\mathbf{u} + \nabla p = \mathbf{f} & \text{in} & \Omega \times (0,T), \\ \nabla\cdot\mathbf{u} = 0 & \text{in} & \Omega \times [0,T), \\ \mathbf{u} = 0 & \text{on} & \partial\Omega \times (0,T), \\ \mathbf{u}(\cdot,0) = \mathbf{u}_0 & \text{in} & \Omega. \end{array}\right. \tag{1}$$

Here, $\nu > 0$ denotes a constant viscosity, $\mathbf{f}$ the source term, and $\mathbf{u}_0 : \Omega \to \mathbb{R}$ the initial velocity field. To derive a weak formulation of (1), the standard spaces for velocity and pressure are defined as follows:

$$\mathbf{V} := H_0^1(\Omega)^d, \quad \text{and} \quad Q := L_0^2(\Omega) = \{q \in L^2(\Omega) : (q,1) = 0\}.$$

Moreover, $\mathbf{L}^2(\Omega) := L^2(\Omega)^d$ denotes the vector-valued L^2 space and $L^2(0,t;X)$ denotes the Bochner space equipped with the norm $\|\cdot\|^2_{L^2(0,t;X)} := \int_0^t \|\cdot(s)\|^2_X ds$. Assuming $\mathbf{f} \in L^2(0,T;\mathbf{L}^2(\Omega))$, $\mathbf{u} \in L^2(0,T;\mathbf{V})$ with $\mathbf{u}_t \in L^2(0,T;\mathbf{L}^2(\Omega))$ and $p \in L^2(0,T;Q)$, the weak solution of the transient Stokes problem (1) fulfills: for all $(\mathbf{v},q) \in L^2(0,T;\mathbf{V}) \times L^2(0,T;Q)$ hold

$$\left\{\begin{array}{rl} (\mathbf{u}_t(t),\mathbf{v}(t)) + \nu(\nabla\mathbf{u}(t),\nabla\mathbf{v}(t)) - (p(t),\nabla\cdot\mathbf{v}(t)) = (\mathbf{f}(t),\mathbf{v}(t)), \\ (q(t),\nabla\cdot\mathbf{u}(t)) = 0, \\ \mathbf{u}(0) = \mathbf{u}_0. \end{array}\right. \tag{2}$$

In order to study the existence and uniqueness of the velocity, the system (2) is usually considered in the space of divergence-free functions

$$\boldsymbol{X}_{\mathrm{div}} := \{\mathbf{v} \in \mathbf{V} : (q,\nabla\cdot\mathbf{v}) = 0 \quad \forall q \in Q\}.$$

Then, a pressure free formulation of the Stokes problem (2) reads: Find $\mathbf{u}(t) \in \boldsymbol{X}_{\mathrm{div}}$ with $\mathbf{u}(0) = \mathbf{u}_0$ such that for almost all $t \in (0,T)$

$$(\mathbf{u}_t(t),\mathbf{v}) + \nu(\nabla\mathbf{u}(t),\nabla\mathbf{v}) = (\mathbf{f}(t),\mathbf{v}) \quad \text{for all } \mathbf{v} \in \boldsymbol{X}_{\mathrm{div}}. \tag{3}$$

2.1 Helmholtz decomposition

The Helmholtz decomposition (see e.g. [22]) states that every vector field $\mathbf{f} \in L^2(\Omega;\mathbb{R}^d)$ can be uniquely decomposed into

$$\mathbf{f} = \nabla\alpha + \boldsymbol{\sigma}$$

with $\alpha \in H^1(\Omega)$ and $\boldsymbol{\sigma} \in L^2_\sigma(\Omega) := \{\mathbf{w} \in H(\mathrm{div}, \Omega) : \nabla \cdot \mathbf{w} = 0, \mathbf{w} \cdot \mathbf{n} = 0 \text{ along } \partial\Omega\}$. In the following, the divergence-free part $\boldsymbol{\sigma} =: \mathbb{P}(\mathbf{f})$ is called the (continuous) Helmholtz projector of $\mathbf{f}$ which can be also written as

$$\mathbb{P}(\mathbf{f}) = \operatorname*{argmin}_{\mathbf{w} \in L^2_\sigma} \|\mathbf{f} - \mathbf{w}\|_0. \tag{4}$$

Note, that the Helmholtz projector of any gradient vanishes, i.e. $\mathbb{P}(\nabla q) = 0$ for all $q \in H^1(\Omega)$ by L^2-orthogonality between gradient fields and $L^2_\sigma(\Omega)$.

2.2 Gronwall's lemma

In the error estimate derivations, the Gronwall's inequality (5) in the form below is applied.

Lemma 2.1 (Gronwall's lemma [27]). *Let $x \in W^{1,1}(0,T)$ and $\Psi, \chi, \lambda \in L^1(0,T)$ and $\Psi(s)$, $\chi(s)$, $\lambda(s) \geq 0$ for almost all $s \in [0,T]$. Assume that on $(0,T)$, it holds*

$$\frac{dx(s)}{ds} + \Psi(s) \leq \chi(s) + \lambda(s)x(s) \quad \textit{for almost all } s \in (0,T).$$

Then, for almost all $t \in [0,T]$ there holds

$$x(t) + \int_0^t \Psi(s)\, ds \leq \exp\left(\int_0^t \lambda(s)\, ds\right)\left(x(0) + \int_0^t \chi(s)\, ds\right). \tag{5}$$

3 Space discretization

Let $\mathbf{V}_h \subset \mathbf{V}$ and $Q_h \subset Q$ denote a pair of finite element spaces corresponding to the shape-regular triangulations $\mathcal{T}_h$ of Ω that satisfy the discrete inf-sup condition

$$\inf_{q_h \in Q_h \setminus \{0\}} \sup_{\mathbf{v}_h \in \mathbf{V}_h \setminus \{0\}} \frac{(\nabla \cdot \mathbf{v}_h, q_h)}{\|\nabla \mathbf{v}_h\|_0 \|q_h\|_0} \geq \beta_h \geq \beta_0 > 0 \tag{6}$$

as $h \to 0$, where h is maximal diameter of the mesh cell $K \in \mathcal{T}_h$. The space of discretely divergence-free functions is defined by

$$\boldsymbol{X}_{h,\mathrm{div}} := \{\mathbf{v}_h \in \mathbf{V}_h : (q_h, \nabla \cdot \mathbf{v}_h) = 0 \quad \forall q_h \in Q_h\}.$$

In this sense, the choice of the finite element pair defines a discrete divergence operator by

$$\nabla_h \cdot \mathbf{v}_h := \operatorname*{argmin}_{q_h \in Q_h} \|\nabla \cdot \mathbf{v}_h - q_h\|_{L^2(\Omega)}.$$

Note, that $\nabla_h \cdot \mathbf{v}_h = 0$ does not imply $\nabla \cdot \mathbf{v}_h = 0$ which is in fact the reason for the lack of pressure-robustness in all classical non-divergence-free schemes. This can be further explained with the discrete Helmholtz projector (in analogy to (4)) defined by

$$\mathbb{P}_h(\mathbf{f}) := \operatorname*{argmin}_{\mathbf{v}_h \in \boldsymbol{X}_{h,\mathrm{div}}} \|\mathbf{f} - \mathbf{v}_h\|_{L^2(\Omega)}$$

which approximates the discretely divergence-free part of a force $\mathbf{f}$. If the functions in $\boldsymbol{X}_{h,\mathrm{div}}$ are not really divergence-free, the discrete Helmholtz projector of a gradient $\mathbf{f} = \nabla p$ is not zero, although the

Helmholtz decomposition of ∇p has no divergence-free part. Throughout the paper, this is expressed in the dual norm

$$\|\mathbf{f}\|_{\boldsymbol{X}^\star_{h,\mathsf{div}}} := \sup_{\mathbf{v}_h \in \boldsymbol{X}_{h,\mathsf{div}}\setminus\{0\}} \frac{(\mathbf{f},\mathbf{v}_h)}{\|\nabla \mathbf{v}_h\|_{L^2(\Omega)}}. \tag{7}$$

In fact, it holds

$$\|\mathbb{P}_h(\nabla p)\|_{\boldsymbol{X}^\star_{h,\mathsf{div}}} = \min_{q_h\in Q_h} \sup_{\mathbf{v}_h \in \boldsymbol{X}_{h,\mathsf{div}}\setminus\{0\}} \frac{(p-q_h,\nabla\cdot\mathbf{v}_h)}{\|\nabla \mathbf{v}_h\|_{L^2(\Omega)}} \leq \min_{q_h\in Q_h} \|p-q_h\|_{L^2(\Omega)}, \tag{8}$$

which is the usual pressure best approximation error that appears in the a priori error analysis of classical mixed finite element methods that are not pressure-robust.

3.1 Classical inf-sup FEM

The space-semi-discretized mixed FEM seeks $(\mathbf{u}_h(t), p_h(t)) \in \mathbf{V}_h \times Q_h$ for all $t \in (0,T)$ such that

$$\left\{\begin{aligned} (\mathbf{u}_{h,t}(t),\mathbf{v}_h) + \nu(\nabla\mathbf{u}_h(t),\nabla\mathbf{v}_h) - (p_h(t),\nabla\cdot\mathbf{v}_h) &= (\mathbf{f}(t),\mathbf{v}_h) && \forall \mathbf{v}_h\in\mathbf{V}_h,\\ (q_h,\nabla\cdot\mathbf{u}_h(t)) &= 0 && \forall q_h\in Q_h,\\ \mathbf{u}_h(0) &= \mathbf{u}_h^0 \end{aligned}\right. \tag{9}$$

where $\mathbf{u}_h^0$ is a suitable approximation of the initial velocity $\mathbf{u}_0$ in the finite element space $\mathbf{V}_h$. In the numerical examples of this paper, we focus on the Bernardi–Raugel finite element method and the P_2^{bub} finite element method but the theory is valid for arbitrary inf-sup stable pairs of finite elements. For the Bernardi–Raugel element, $\mathbf{V}_h$ consists of piecewise linear continuous vector-valued polynomials P_1 and additional face bubbles in normal direction and Q_h consists of piecewise constant functions P_0, see [10]. The P_2^{bub} finite element method employs piecewise quadratic continuous vector-valued polynomials plus additional cell bubbles denoted by $\mathbf{V}_h = (P_2^{\mathrm{bub}})^d$ and piecewise linear discontinuous pressure ansatz functions $Q_h = P_1^{\mathrm{disc}}$.

Theorem 3.1. *Let $(\mathbf{u},p)$ be the solution of* (2) *with $\mathbf{u}_t, \Delta\mathbf{u}, \nabla p \in L^2(0,T;\mathbf{L}^2(\Omega))$ and let $(\mathbf{u}_h,p_h)$ be the solution of* (9)*.*

(A) For all $t\in(0,T)$ and arbitrary $\mathbf{w}_h \in L^2(0,t;\boldsymbol{X}_{h,div})$, it holds

$$\begin{aligned} &\|\mathbf{u}(t)-\mathbf{u}_h(t)\|^2_{L^2(\Omega)} + \nu\|\nabla(\mathbf{u}-\mathbf{u}_h)\|^2_{L^2(0,t;L^2)} \leq 2\left[\|(\mathbf{u}-\mathbf{w}_h)(t)\|^2_{L^2(\Omega)} + \nu\|\nabla(\mathbf{u}-\mathbf{w}_h)\|^2_{L^2(0,t;L^2)}\right]\\ &+2\min\Big\{\left(\|\mathbf{w}_h^0-\mathbf{u}_h^0\|^2_{L^2(\Omega)} + \frac{2}{\nu}\|\mathbb{P}_h(\mathbf{w}_{h,t}-\mathbf{u}_t+\nabla p)\|^2_{L^2(0,t;\boldsymbol{X}^\star_{h,div})} + 2\nu\|\nabla(\mathbf{u}-\mathbf{w}_h)\|^2_{L^2(0,t;L^2)}\right),\\ &\exp(1)\left(\|\mathbf{w}_h^0-\mathbf{u}_h^0\|^2_{L^2(\Omega)} + t\|\mathbb{P}_h(\mathbf{w}_{h,t}-\mathbf{u}_t+\nabla p)\|^2_{L^2(0,t;L^2)} + \nu\|\nabla(\mathbf{u}-\mathbf{w}_h)\|^2_{L^2(0,t;L^2)}\right)\Big\}. \end{aligned}$$

(B) If $\mathbf{w}_h$ is the L^2 best approximation of $\mathbf{u}$ in $\boldsymbol{X}_{h,div}$, then statement (A) holds with

$$\mathbb{P}_h(\mathbf{w}_{h,t}-\mathbf{u}_t+\nabla p) = \mathbb{P}_h(\nabla p).$$

Proof of Theorem 3.1 (A). For fixed $\mathbf{e}_h = \mathbf{u}_h - \mathbf{w}_h \in L^2(0,t;\boldsymbol{X}_{h,\mathsf{div}})$, the error equation is obtained by subtracting (2) from (9), i.e., for almost all $s\in(0,t)$ it holds

$$\begin{aligned} &((\mathbf{u}_{h,t}-\mathbf{w}_{h,t})(s),\mathbf{e}_h(s)) + \nu(\nabla(\mathbf{u}_h-\mathbf{w}_h)(s),\nabla\mathbf{e}_h(s))\\ &\qquad = ((\mathbf{u}_t-\mathbf{w}_{h,t})(s),\mathbf{e}_h(s)) + \nu(\nabla(\mathbf{u}-\mathbf{w}_h)(s),\nabla\mathbf{e}_h(s)) + (\nabla p(s),\mathbf{e}_h(s))\\ &\qquad = (\mathbb{P}_h(\mathbf{u}_t-\mathbf{w}_{h,t}+\nabla p)(s),\mathbf{e}_h(s)) + \nu(\nabla(\mathbf{u}-\mathbf{w}_h)(s),\nabla\mathbf{e}_h(s)). \end{aligned}$$

Then, the Cauchy–Schwarz and Young inequalities applied to the right-hand side lead to

$$\begin{aligned}\frac{1}{2}\frac{d}{ds}\|\mathbf{e}_h(s)\|^2_{L^2(\Omega)} + \frac{\nu}{2}\|\nabla \mathbf{e}_h(s)\|^2_{L^2(\Omega)} \\ \leq \min\Bigg\{ \left(\frac{1}{\nu}\|\mathbb{P}_h(\mathbf{u}_t - \mathbf{w}_{h,t} + \nabla p)(s)\|^2_{\boldsymbol{X}^\star_{h,\mathsf{div}}} + \nu\|\nabla(\mathbf{w}_h - \mathbf{u})(s)\|^2_{L^2(\Omega)}\right), \\ \left(\frac{t}{2}\|\mathbb{P}_h(\mathbf{u}_t - \mathbf{w}_{h,t} + \nabla p)(s)\|^2_{L^2(\Omega)} + \frac{1}{2t}\|\mathbf{e}_h(s)\|^2_{L^2(\Omega)} + \frac{\nu}{2}\|\nabla(\mathbf{w}_h - \mathbf{u})(s)\|^2_{L^2(\Omega)}\right)\Bigg\}.\end{aligned}$$

Integrating this estimate over 0 to t in the first case, applying the Gronwall Lemma 2.1 with $\lambda(s) = 1/t$ in the second case, and applying a triangle inequality conclude the proof. □

Proof of Theorem 3.1 (B). This follows directly from the fact that the time derivative and the application of the projection $\mathbb{P}_h$ commute and that $\mathbf{w}_h$ is the L^2 best approximation of $\mathbf{u}$ in $\boldsymbol{X}_{h,\mathsf{div}}$, i.e. $\mathbf{w}_h = \mathbb{P}_h(\mathbf{u})$. Hence,

$$\mathbb{P}_h(\mathbf{u}_t - \mathbf{w}_{h,t} + \nabla p) = \frac{d}{dt}(\mathbb{P}_h(\mathbf{u}) - \mathbf{w}_h) + \mathbb{P}_h(\nabla p) = \mathbb{P}_h(\nabla p).$$

□

Remark 3.2. *Theorem 3.1.(B) shows that classical mixed methods for the transient incompressible Stokes equations are not really locking-free, since $\nu^{-1}\|\mathbb{P}_h(\nabla p)\|_{L^2(0,t;\boldsymbol{X}^\star_{h,div})}$ can be possibly large. Alternatively, $t\|\mathbb{P}_h(\nabla p)\|_{L^2(0,t;L^2)}$ can exceed every bound for large t. The reason for such possibly large errors is just the lack of L^2 orthogonality between discretely divergence-free vector fields and gradient fields in the momentum balance, which are balanced by the pressure gradient. The estimates above are sharp. We demonstrate this by some simple hydrostatic model problems, which can be explicitly solved. Denoting by M_h, Δ_h and $\mathcal{P}_h$ the representation matrices for the FEM mass matrix, the discrete vector Laplacian and the L^2 projector onto the discretely divergence-free vector fields, we investigate model problems for* (2) *with a right hand side $\mathbf{f} = \nabla\phi$ with $\phi \in C^\infty(\Omega) \cap Q \wedge \phi \notin Q_h$ such that $\mathbb{P}_h(\nabla\phi) \neq \mathbf{0}$. If not all vector fields in $\boldsymbol{X}_{h,div}$ are divergence-free, then such a ϕ always exists, according to the (continuous) Helmholtz decomposition. Then, for all times $t > 0$ the continuous solution of this hydrostatic problem is just $(\mathbf{u}, p) = (\mathbf{0}, \phi)$. However, the discrete velocity solution $\mathbf{u}_h$ of* (9) *is non-zero and can be easily characterized. Defining $\mathbf{g}_h := \mathbb{P}_h(\nabla\phi) = \mathbb{P}_h(\nabla p) \in \boldsymbol{X}_{h,div}$, for the vanishing viscosity case $\nu = 0$ the velocity solution is just $\mathbf{u}_h(t) = t(\mathcal{P}_h^T M_h \mathcal{P}_h)^{-1}\mathbf{g}_h$, which shows the sharpness of the Gronwall-type estimate. For $\nu > 0$ the discrete velocity solution converges for $t \to \infty$ to a discrete steady solution, which can be described as $\mathbf{u}_h^\infty = \frac{1}{\nu}(\mathcal{P}_h^T\Delta_h\mathcal{P}_h)^{-1}\mathbf{g}_h$ and shows the sharpness of the ν^{-1}-dependent estimate. Indeed, for all $t > 0$ one gets $\mathbf{u}_h(t) = (I - \exp(-\nu C_h t))\mathbf{u}_h^\infty$ with the identity matrix I and $C_h = (\mathcal{P}_h^T M_h \mathcal{P}_h)^{-1}(\mathcal{P}_h^T\Delta_h\mathcal{P}_h)$. Expanding the matrix series, yields $\mathbf{u}_h(t) = t(\mathcal{P}_h^T M_h \mathcal{P}_h)^{-1}\mathbf{g}_h - \frac{1}{2}\nu t^2 C_h\mathbf{g}_h + \ldots$, which shows that the Gronwall type estimate is sharper for short time computations, and the ν^{-1}-dependent estimate is sharper for long time computations. In a nutshell, one can say that the main problem of classical mixed methods for the transient incompressible Stokes equations is that they are not able to handle correctly general hydrostatic flow problems (i.e, whenever it holds $\phi \notin Q_h$).*

Remark 3.3. *Despite locking effects due to small viscosities $0 < \nu \ll 1$, Theorem 3.1 shows at least asymptotically optimal convergence. Indeed, assuming enough regularity for $\mathbf{u}$ and p, one can choose, for almost all $s \in (0,t)$, $\mathbf{w}_h(s)$ as the (space) best approximation in the H^1-semi norm. $\|\mathbb{P}_h(\nabla p)\|_{L^2(0,t;\boldsymbol{X}^\star_{h,div})}$ has the optimal rate, anyway, see* (8).

3.2 Pressure-Robust FEM

In this section, the weak form (2) is discretized in space by a modified pressure-robust mixed finite element method that employs a reconstruction operator Π with two important properties.

First, it maps discretely divergence-free functions onto divergence-free test functions. This also implies a modified discrete Helmholtz projector defined by

$$\mathbb{P}_h^\star(\mathbf{f}) := \operatorname*{argmin}_{\mathbf{v}_h \in \Pi \boldsymbol{X}_{h,\mathrm{div}}} \|\mathbf{f} - \Pi \mathbf{v}_h\|_{L^2(\Omega)}.$$

This modification of the discrete Helmholtz projector leads to the fact that the discrete Helmholtz projection is zero when applied to gradients, i.e., L^2-orthogonality of the operator $\Pi \boldsymbol{X}_{\mathrm{div}}^0$ onto gradients of H^1-functions is established [32, 34]. This property ensures the pressure-independence of the a priori error estimates.

Second, the velocity reconstruction operator Π for any pressure-robust finite element method of order k satisfies some consistency error estimate in the abstract form

$$(\mathbf{g}, \mathbf{v}_h - \Pi \mathbf{v}_h) \leq C h^k |\mathbf{g}|_{k-1} \|\nabla \mathbf{v}_h\|_{L^2(\Omega)} \quad \text{for any } \mathbf{g} \in H^{k-1}(\Omega)^d. \tag{10}$$

This property ensures that the modified method still converges with the optimal order. In particular, for $\mathbf{u} \in H^{k+1}(\Omega)^d$, it follows

$$\|\Delta \mathbf{u} \circ (1 - \Pi)\|_{\boldsymbol{X}_{h,\mathrm{div}}^\star} := \sup_{\mathbf{v}_h \in \boldsymbol{X}_{h,\mathrm{div}} \setminus \{0\}} \frac{(\Delta \mathbf{u}, \mathbf{v}_h - \Pi \mathbf{v}_h)}{\|\nabla \mathbf{v}_h\|_{L^2(\Omega)}} \leq C h^k |\mathbf{u}|_{k+1}. \tag{11}$$

Moreover, similar to (7) the error analysis for the modified method involves dual norms of the type

$$\|\mathbf{g} \circ \Pi\|_{\boldsymbol{X}_{h,\mathrm{div}}^\star} := \sup_{\mathbf{v}_h \in \boldsymbol{X}_{h,\mathrm{div}} \setminus \{0\}} \frac{(\mathbf{g}, \Pi \mathbf{v}_h)}{\|\nabla \mathbf{v}_h\|_{L^2(\Omega)}}. \tag{12}$$

A triangle inequality and similar arguments as above show the estimate

$$\|\mathbf{g} \circ \Pi\|_{\boldsymbol{X}_{h,\mathrm{div}}^\star} \leq \|\mathbf{g}\|_{\boldsymbol{X}_{h,\mathrm{div}}^\star} + \|\mathbf{g} \circ (1 - \Pi)\|_{\boldsymbol{X}_{h,\mathrm{div}}^\star} = \|\mathbf{g}\|_{\boldsymbol{X}_{h,\mathrm{div}}^\star} + C h^s |\mathbf{g}|_{s-1} \tag{13}$$

where $s \leq k$ is the regularity of $\mathbf{g} \in H^{s-1}(\Omega)$. Usually this is only needed for $s = 1$, i.e., $\mathbf{g} \in L^2(\Omega)^d$ to get a higher-order perturbation of the original dual norm in the classical estimates.

Reconstruction operators with these properties are available for many classical finite element methods, e.g. for the Bernardi–Raugel finite element method [34] or others with discontinuous pressure elements [32, 35, 36]. There, standard interpolation operators into Brezzi–Douglas–Marini or Raviart-Thomas spaces can be employed that naturally satisfy (10), see e.g. [3]. Recently, also for the popular Taylor–Hood and mini finite element method a reconstruction operator with these properties was designed [30].

The reconstruction operator Π is applied to the test-functions only in the right-hand side and in the time-derivative. This leads to the pressure-robust mixed FEM that reads: For all $t \in (0, T)$, find $(\mathbf{u}(t), p(t)) \in \mathbf{V}_h \times Q_h$ such that

$$\begin{cases} (\Pi \mathbf{u}_{h,t}, \Pi \mathbf{v}_h) + \nu(\nabla \mathbf{u}_h, \nabla \mathbf{v}_h) - (p_h, \nabla \cdot \mathbf{v}_h) = (\mathbf{f}, \Pi \mathbf{v}_h) & \forall \mathbf{v}_h \in \mathbf{V}_h, \\ (q_h, \nabla \cdot \mathbf{u}_h) = 0 & \forall q_h \in Q_h, \\ \mathbf{u}_h(0) = \mathbf{u}_h^0. \end{cases} \tag{14}$$

This discretization is only semi-discrete with respect to space, but not discrete in time. The fully discrete scheme is studied below in Section 5. The following assumption is essential, in order to show optimal convergence orders for the pressure-robust discretization.

Assumption 3.4. *For the velocity reconstruction operator, the kernel of* $\Pi : \boldsymbol{X}_{h,div} \to \Pi(\boldsymbol{X}_{h,div})$ *is denoted by* $\ker(\Pi)$*. Denoting* $\ker(\Pi)^\perp$ *as the orthogonal complement of* $\ker(\Pi)$ *in* $\boldsymbol{X}_{h,div}$ *with respect to the scalar product* $(\nabla\bullet, \nabla\bullet)$*, we assume*

$$C_1\|\mathbf{v}_h\|_{L^2(\Omega)} \leq \|\Pi\mathbf{v}_h\|_{L^2(\Omega)} \leq C_2\|\mathbf{v}_h\|_{L^2(\Omega)} \quad \text{for all } \mathbf{v}_h \in \ker(\Pi)^\perp, \tag{15}$$

where C_1 *and* C_2 *denote constants, which depends on the shape-regularity of the mesh, but not on the mesh size.*

Remark 3.5. *The first inequality of* (15) *follows in a generic way, even for all* $\mathbf{v}_h \in \boldsymbol{X}_{h,div}$*, from the* (10) *and an inverse inequality by*

$$\|\Pi\mathbf{v}_h\|_{L^2(\Omega)} \leq \|\mathbf{v}_h\|_{L^2(\Omega)} + \|\mathbf{v}_h - \Pi\mathbf{v}_h\|_{L^2(\Omega)} \leq \|\mathbf{v}_h\|_{L^2(\Omega)} + Ch\|\nabla\mathbf{v}_h\|_{L^2(\Omega)} \leq \tilde{C}\|\mathbf{v}_h\|_{L^2(\Omega)}.$$

The second inequality needs a detailed investigation of the the used mixed finite element method and the used reconstruction operator. We checked this condition numerically for the used discretizations from the numerical section, which requires essentially the numerical solution of a generalized eigenvalue problem.

Theorem 3.6. *Let* $(\mathbf{u}, p)$ *be the solution of* (2) *with* $\mathbf{u}_t, \Delta\mathbf{u}, \nabla p \in L^2(0,T;\mathbf{L}^2(\Omega))$*, and let* $(\mathbf{u}_h, p_h)$ *be the solution of* (9)*.*

(A*) For all* $t \in (0,T)$ *with arbitrary* $\mathbf{w}_h \in L^2(0,t;\boldsymbol{X}_{h,div})$*, it holds*

$$\begin{aligned}
\|(\mathbf{u}-\Pi\mathbf{u}_h)(t)\|^2_{L^2(\Omega)} + \nu\|\nabla(\mathbf{u}-\mathbf{u}_h)\|^2_{L^2(0,t;L^2)} &\leq 2\Big[\|(\mathbf{u}-\Pi\mathbf{w}_h)(t)\|^2_{L^2(\Omega)} + \nu\|\nabla(\mathbf{u}-\mathbf{w}_h)\|^2_{L^2(0,t;L^2)}\Big] \\
+2\min\Bigg\{\Bigg(&\|\Pi(\mathbf{w}_h^0-\mathbf{u}_h^0)\|^2_{L^2(\Omega)} + 3\nu\|\Delta\mathbf{u}\circ(1-\Pi)\|^2_{L^2(0,t;\boldsymbol{X}^\star_{h,div})} + \frac{3}{\nu}\|\mathbb{P}^\star_h(\mathbf{u}_t-\Pi\mathbf{w}_{h,t})\circ\Pi\|^2_{L^2(0,t;\boldsymbol{X}^\star_{h,div})} \\
&+ 3\nu\|\nabla(\mathbf{u}-\mathbf{w}_h)\|^2_{L^2(0,t;L^2)}\Bigg), \\
\exp(1)\Bigg(&\|\Pi(\mathbf{w}_h^0-\mathbf{u}_h^0)\|^2_{L^2(\Omega)} + 2\nu\|\Delta\mathbf{u}\circ(1-\Pi)\|^2_{L^2(0,t;\boldsymbol{X}^\star_{h,div})} + t\|\mathbb{P}^\star_h(\mathbf{u}_t-\Pi\mathbf{w}_{h,t})\|^2_{L^2(0,t;L^2)} \\
&+ 2\nu\|\nabla(\mathbf{u}-\mathbf{w}_h)\|^2_{L^2(0,t;L^2)}\Bigg)\Bigg\}.
\end{aligned}$$

(B*) If* $\Pi\mathbf{w}_h$ *is chosen as the* L^2 *best approximation of* $\mathbf{u}$ *in* $\Pi(\boldsymbol{X}_{h,div})$*, then statement* (A) *holds with*

$$\mathbb{P}^\star_h(\mathbf{u}_t - \Pi\mathbf{w}_{h,t}) = 0,$$

yielding a locking-free error estimate.

(C*) For almost all* $t \in (0,T)$ *and* $\pi_{Q_h}p$ *denoting the* L^2 *best approximation of* p *in* Q_h*, it holds*

$$\begin{aligned}
\|(\pi_{Q_h}p - p_h)(t)\|_{L^2(\Omega)} \leq \frac{1}{\beta_0}\big(&\|\mathbb{P}^\star_h(\mathbf{u}_t - \Pi\mathbf{u}_{h,t})(t)\circ\Pi\|_{\boldsymbol{X}^\star_{h,div}} + \nu\|\Delta\mathbf{u}(t)\circ(1-\Pi)\|_{\boldsymbol{X}^\star_{h,div}} \\
&+ \nu\|\nabla(\mathbf{u}-\mathbf{u}_h)(t)\|_{L^2(\Omega)}\big).
\end{aligned}$$

Proof of Theorem 3.6.(A*).* Subtracting (2) from (14) and testing with $\mathbf{v}_h \in L^2(0,t;\boldsymbol{X}_{h,\mathrm{div}})$, one gets

$$((\Pi\mathbf{u}_{h,t} - \mathbf{u}_t)(s), \Pi\mathbf{v}_h(s)) + \nu(\nabla(\mathbf{u}_h - \mathbf{u})(s), \nabla\mathbf{v}_h(s)) - \nu(\Delta\mathbf{u}, \mathbf{v}_h(s) - \Pi\mathbf{v}_h(s)) = \mathbf{0}$$

for almost all $s \in (0,t)$. Here, we used the decisive property of the velocity reconstruction operator Π in pressure-robust mixed methods that $(\nabla p, \Pi\mathbf{v}_h) = \mathbf{0}$ holds for all $\mathbf{v}_h \in \boldsymbol{X}_{h,\mathrm{div}}$ [32, 36, 30]. Using

$\mathbf{f} - \mathbf{u}_t = -\nu\Delta\mathbf{u} + \nabla p$ together with fixed $\mathbf{e}_h := \mathbf{u}_h - \mathbf{w}_h \in L^2(0,t;\boldsymbol{X}_{h,\mathsf{div}})$ and a straightforward calculation with $\mathbf{v}_h = \mathbf{e}_h$ leads to

$$\begin{aligned}&\frac{1}{2}\frac{d}{ds}\|\Pi\mathbf{e}_h(s)\|^2_{L^2(\Omega)} + \nu\|\nabla\mathbf{e}_h(s)\|^2_{L^2(\Omega)}\\ &\quad= ((\mathbf{u}_t - \Pi\mathbf{w}_{h,t})(s), \Pi\mathbf{e}_h(s)) + \nu(\Delta\mathbf{u}(s), (\mathbf{e}_h - \Pi\mathbf{e}_h)(s)) + \nu(\nabla(\mathbf{u}-\mathbf{w}_h)(s), \nabla\mathbf{e}_h(s)).\end{aligned}$$

Applying the Cauchy–Schwarz and Young's inequality to the first term on the right-hand side and using the consistency error (11) gives

$$\begin{aligned}&\frac{1}{2}\frac{d}{ds}\|\Pi\mathbf{e}_h(s)\|^2_{L^2(\Omega)} + \frac{\nu}{2}\|\nabla\mathbf{e}_h(s)\|^2_{L^2(\Omega)} \le \min\left\{\left(\frac{3}{2\nu}\|\mathbb{P}^\star_h(\mathbf{u}_t - \Pi\mathbf{w}_{h,t})(s)\circ\Pi\|^2_{\boldsymbol{X}^\star_{h,\mathsf{div}}}\right.\right.\\ &+ \frac{3\nu}{2}\|\Delta\mathbf{u}(s)\circ(1-\Pi)\|^2_{\boldsymbol{X}^\star_{h,\mathsf{div}}} + \frac{3\nu}{2}\|\nabla(\mathbf{u}-\mathbf{w}_h)(s)\|^2_{L^2(\Omega)}\Big), \Big(\frac{t}{2}\|\mathbb{P}^\star_h(\mathbf{u}_t - \Pi\mathbf{w}_{h,t})(s)\|^2_{L^2(\Omega)}\\ &\qquad\left.\left.+ \frac{1}{2t}\|\Pi\mathbf{e}_h(s)\|^2_{L^2(\Omega)} + \nu\|\Delta\mathbf{u}(s)\circ(1-\Pi)\|^2_{\boldsymbol{X}^\star_{h,\mathsf{div}}} + \nu\|\nabla(\mathbf{u}-\mathbf{w}_h)(s)\|^2_{L^2(\Omega)}\Big)\right\}.\end{aligned}$$

Note that, the $\|\nabla\mathbf{e}_h(s)\|^2_{L^2(\Omega)}$-norms were absorbed in the left-hand side. Then, the inequality is integrated over the time 0 to t in the first min case, or the Gronwall Lemma 2.1 with $\lambda(s) = 1/t$ is applied in the second min case. This leads to

$$\begin{aligned}&\|\Pi\mathbf{e}_h(t)\|^2_{L^2(\Omega)} + \nu\|\nabla\mathbf{e}_h\|^2_{L^2(0,t;L^2)} \le \min\left\{\left(\|\Pi(\mathbf{w}^0_h - \mathbf{u}^0_h)\|^2_{L^2(\Omega)} + 3\nu\|\Delta\mathbf{u}\circ(1-\Pi)\|^2_{L^2(0,t;\boldsymbol{X}^\star_{h,\mathsf{div}})}\right.\right.\\ &+ \frac{3}{\nu}\|\mathbb{P}^\star_h(\mathbf{u}_t - \Pi\mathbf{w}_{h,t})\circ\Pi\|^2_{L^2(0,t;\boldsymbol{X}^\star_{h,\mathsf{div}})} + 3\nu\|\nabla(\mathbf{u}-\mathbf{w}_h)\|^2_{L^2(0,t;L^2)}\Big), \exp(1)\Big(\|\Pi(\mathbf{w}^0_h - \mathbf{u}^0_h)\|^2_{L^2(\Omega)}\\ &\left.\left.+ 2\nu\|\Delta\mathbf{u}\circ(1-\Pi)\|^2_{L^2(0,t;\boldsymbol{X}^\star_{h,\mathsf{div}})} + t\|\mathbb{P}^\star_h(\mathbf{u}_t - \Pi\mathbf{w}_{h,t})\|^2_{L^2(0,t;L^2)} + 2\nu\|\nabla(\mathbf{u}-\mathbf{w}_h)\|^2_{L^2(0,t;L^2)}\Big)\right\}.\end{aligned}$$

The statement follows by a triangle inequality and $(\|a\| + \|b\|)^2 \le 2\|a\|^2 + 2\|b\|^2$. □

Proof of Theorem 3.6.(B). The proof is similar to the proof of Theorem 3.1.(B). □

Proof of Theorem 3.6.(C). As in the steady case (see e.g. [32, 36]), the operator Π satisfies $\nabla_h\cdot\mathbf{v}_h = \nabla_h\cdot(\Pi\mathbf{v}_h)$ for any $\mathbf{v}_h \in \mathbf{V}_h$. This and $(\pi_{Q_h}p(t), \nabla\cdot\mathbf{v}_h) = (p(t), \nabla\cdot\mathbf{v}_h)$ plus similar arguments as in (A) yield

$$\begin{aligned}((\pi_{Q_h}p - p_h)(t), \nabla\cdot\mathbf{v}_h) = (\mathbb{P}^\star_h(\mathbf{u}_t - \mathbf{u}_{h,t})(t), \Pi\mathbf{v}_h) + \nu(\Delta\mathbf{u}(t), \mathbf{v}_h - \Pi\mathbf{v}_h)\\ + \nu(\nabla(\mathbf{u}-\mathbf{u}_h)(t), \nabla\mathbf{v}_h).\end{aligned}$$

The inf-sup stability guarantees that $v_h \in \mathbf{V}_h$ exists with

$$\nabla\cdot\mathbf{v}_h = (\pi_{Q_h}p - p_h)(t) \quad\text{and}\quad \|\nabla\mathbf{v}_h\|_{L^2(\Omega)} \le \frac{1}{\beta_0}\|(\pi_{Q_h}p - p_h)(t)\|_{L^2(\Omega)}.$$

The combination of both arguments and Cauchy–Schwarz inequality conclude the proof. □

Remark 3.7. *According to our estimates, a reasonable choice for the initial value in numerical simulations $\mathbf{u}^0_h$ is such that $\Pi\mathbf{w}_h(0)$ is the best approximation in L^2 of the continuous initial value $\mathbf{u}_0$ within the space of divergence-free vector fields $\Pi(\boldsymbol{X}_{h,div})$.*

Remark 3.8. *The choice of $\Pi\mathbf{w}_h$ (and therefore of $\mathbf{w}_h$) in Theorem 3.6.(B) leads to a locking-free estimate in the sense that the estimate is independent of ν^{-1} for $0 < \nu \ll 1$. However, it is also important to know the convergence order of the method with this choice, of course. For this objective, the pressure-robust mixed method together with its velocity reconstruction operator has to be investigated in detail.*

i) The distance of $\mathbf{w}_h$ to the L^2 best approximation $\tilde{\mathbf{w}}_h$ of $\mathbf{u}$ in $\mathrm{Ker}(\Pi)^\perp \subset \boldsymbol{X}_{h,div}$ can be estimated by

$$\begin{aligned}\|\Pi\mathbf{w}_h - \Pi\tilde{\mathbf{w}}_h\|^2_{L^2(\Omega)} &= (\Pi\mathbf{u} - \Pi\tilde{\mathbf{w}}_h, \Pi\mathbf{w}_h - \Pi\tilde{\mathbf{w}}_h)\\ &\leq \|\Pi\mathbf{u} - \Pi\tilde{\mathbf{w}}_h\|_{L^2(\Omega)}\|\Pi\mathbf{w}_h - \Pi\tilde{\mathbf{w}}_h\|_{L^2(\Omega)}\\ &\leq \big(Ch\|\nabla(\mathbf{u} - \tilde{\mathbf{w}}_h)\|_{L^2(\Omega)} + \|\mathbf{u} - \tilde{\mathbf{w}}_h\|_{L^2(\Omega)}\big)\,\|\Pi\mathbf{w}_h - \Pi\tilde{\mathbf{w}}_h\|_{L^2(\Omega)}\end{aligned}$$

Under the assumption (15) *and standard arguments on shape-regular meshes like inverse inequalities, one gets*

$$h\|\nabla(\mathbf{w}_h - \tilde{\mathbf{w}}_h)\|_{L^2(\Omega)} \lesssim \|\mathbf{w}_h - \tilde{\mathbf{w}}_h\|_{L^2(\Omega)} \lesssim \|\Pi\mathbf{w}_h - \Pi\tilde{\mathbf{w}}_h\|_{L^2(\Omega)}$$

For all the used mixed discretizations and the corresponding reconstruction operators in the numerical section, this result delivers optimal $k+1$ order convergence. In these cases, the kernels of the reconstruction operators are empty, and $\tilde{w}_h$ is just the L^2 best approximation in $\boldsymbol{X}_{h,div}$. Then, $\|\mathbf{u}-\tilde{\mathbf{w}}_h\|_{L^2(\Omega)}$ and $Ch\|\nabla(\mathbf{u}-\tilde{\mathbf{w}}_h)\|_{L^2(\Omega)}$ converge with optimal order $k+1$ on convex domains. Therefore, $\|\nabla(\mathbf{u}-\mathbf{w}_h)\|_{L^2(\Omega)}$ converges with optimal order k.

ii) It remains to investigate the approximation error $\|(\mathbf{u} - \Pi\mathbf{w}_h)(t)\|_{L^2(\Omega)}$, which depends on the approximation properties of $\Pi\boldsymbol{X}_{h,div} \subset L^2_\sigma(\Omega)$. Similarly as above, one estimates

$$\|\mathbf{u} - \Pi\mathbf{w}_h\|_{L^2(\Omega)} \leq \|\mathbf{u} - \Pi\mathbf{u}\|_{L^2(\Omega)} + \|\Pi(\mathbf{u} - \tilde{\mathbf{w}}_h)\|_{L^2(\Omega)} + \|\Pi(\tilde{\mathbf{w}_h} - \mathbf{w}_h)\|_{L^2(\Omega)}.$$

Since $\|\mathbf{u} - \Pi\mathbf{u}\|_{L^2(\Omega)}$ and $\|\Pi(\tilde{\mathbf{w}_h} - \mathbf{w}_h)\|_{L^2(\Omega)}$ converge with optimal orders, it remains to estimate

$$\|\Pi(\mathbf{u} - \tilde{\mathbf{w}}_h)\|_{L^2(\Omega)} \leq \|\mathbf{u} - \tilde{\mathbf{w}}_h\|_{L^2(\Omega)} + Ch\|\nabla(\mathbf{u} - \tilde{\mathbf{w}}_h)\|_{L^2(\Omega)}.$$

Again, by standards arguments on shape-regular meshes the optimal convergence order is proved.

Remark 3.9. *The statement (C) in Theorem 3.6 shows a certain pressure-robustness of the pressure error, as it is known for pressure-robust discretizations of the steady Stokes problem [36]. Indeed, the discrete pressure at every time is the best approximation of the continuous pressure in L^2 up to an error, which is only velocity-dependent. In [34] it is shown that for time-dependent potential flows, the improved space discretization of the time derivate $(\Pi\mathbf{u}_{h,t}, \Pi\mathbf{v}_h)$ allows sometimes much larger time steps than the classical discretization $(\mathbf{u}_{h,t}, \mathbf{v}_h)$ without affecting the local-in-time velocity error. Theorem 3.6 shows that also the local-in-time pressure error will not be affected negatively, since it just follows the velocity error.*

4 Limit case

For $\nu \to 0$ our model problem approaches the problem

$$\mathbf{u}_t + \nabla p = \mathbf{f} \quad \text{and} \quad \nabla \cdot \mathbf{u} = 0.$$

For this limit case some improved error estimates can be proven.

Theorem 4.1. *Let $(\mathbf{u}, p)$ be the solution of* (2) *with $\mathbf{u}_t, \nabla p \in L^2(0,T;\mathbf{L}^2(\Omega))$.*

(A) For the classical discretization (9) *with* $\nu = 0$*, it holds, for almost all* $t \in (0,T)$*,*

$$\|\mathbf{u}(t) - \mathbf{u}_h(t)\|^2_{L^2(\Omega)} \leq \inf_{\mathbf{w}_h \in \boldsymbol{X}_{h,div}} \|\mathbf{u}(t) - \mathbf{w}_h\|^2_{L^2(\Omega)} + \left(\|\mathbf{u}(0) - \mathbf{u}_h(0)\|_{L^2(\Omega)} + \| \int_0^t \mathbb{P}_h(\nabla p(s))\, ds \|_{L^2(\Omega)} \right)^2.$$

(B) For the pressure-robust discretization (14) *with* $\nu = 0$*, it holds, for almost all* $t \in (0,T)$*,*

$$\|\mathbf{u}(t) - \Pi\mathbf{u}_h(t)\|^2_{L^2(\Omega)} \leq \inf_{\mathbf{w}_h \in \boldsymbol{X}_{h,div}} \|\mathbf{u}(t) - \Pi\mathbf{w}_h\|^2_{L^2(\Omega)} + \|\mathbf{u}(0) - \Pi\mathbf{u}_h(0)\|^2_{L^2(\Omega)}.$$

In other words, the solution of the pressure-robust scheme $\Pi\mathbf{u}_h(t)$ *equals the* L^2 *best approximation in* $\Pi\boldsymbol{X}_{h,div}$ *of* $\mathbf{u}(t)$ *up to some initial error. Moreover, (B) and (C) of Theorem 3.6 also show that* p_h *is the* L^2 *best approximation of* p *for almost all* $t \in (0,T)$*.*

Similarly, a fully divergence-free method (like the Scott–Vogelius finite element method where $\mathbb{P}_h = \mathbb{P}$ *with* $\Pi = 1$*) gives the best approximation in* $\boldsymbol{X}_{h,div}$ *up to some initial error.*

Proof of (A). Subtracting the continuous problem (2) from the classical discrete problem (9) for $\nu = 0$ and $s \in (0,t)$ and inserting $\mathbf{f}(s) = \mathbf{u}_t(s) + \nabla p(s)$ gives

$$\frac{d}{dt}(\mathbf{u}(s) - \mathbf{u}_h(s), \mathbf{v}_h) = -(\nabla p(s), \mathbf{v}_h) = -(\mathbb{P}_h \nabla p(s), \mathbf{v}_h).$$

for any (time-independent) test function $\mathbf{v}_h \in \boldsymbol{X}_{h,\mathrm{div}}$. Integration over $(0,t)$ gives

$$\begin{aligned}(\mathbf{u}(t) - \mathbf{u}_h(t), \mathbf{v}_h) &= (\mathbf{u}(0) - \mathbf{u}_h(0), \mathbf{v}_h) - \int_0^t (\mathbb{P}_h \nabla p(s), \mathbf{v}_h)\, ds \\ &= (\mathbf{u}(0) - \mathbf{u}_h(0), \mathbf{v}_h) - (\int_0^t \mathbb{P}_h \nabla p(s)\, ds, \mathbf{v}_h) \\ &\leq \left(\|\mathbf{u}(0) - \mathbf{u}_h(0)\|_{L^2(\Omega)} + \| \int_0^t \mathbb{P}_h(\nabla p(s))\, ds \|_{L^2(\Omega)} \right) \|\mathbf{v}_h\|_{L^2(\Omega)}.\end{aligned}$$

The best approximation $\mathbf{w}_h$ of $\mathbf{u}(t)$ in $\boldsymbol{X}_{h,\mathrm{div}}$ is characterized by

$$(\mathbf{w}_h - \mathbf{u}(t), \mathbf{v}_h) = 0 \quad \text{for all } \mathbf{v}_h \in \boldsymbol{X}_{h,\mathrm{div}}.$$

Hence, testing with the test function $\mathbf{v}_h := \mathbf{u}_h(t) - \mathbf{w}_h \in \boldsymbol{X}_{h,\mathrm{div}}$ gives

$$\begin{aligned}\|\mathbf{v}_h\|^2_{L^2(\Omega)} &= \|\mathbf{w}_h - \mathbf{u}_h(t)\|^2_{L^2(\Omega)} \\ &= (\mathbf{w}_h - \mathbf{u}(t), \mathbf{v}_h) + (\mathbf{u}(t) - \mathbf{u}_h(t), \mathbf{v}_h) \\ &\leq \left(\|\mathbf{u}(0) - \mathbf{u}_h(0)\|_{L^2(\Omega)} + \int_0^t \|\mathbb{P}_h(\nabla p(s))\|_{L^2(\Omega)}\, ds \right) \|\mathbf{v}_h\|_{L^2(\Omega)}.\end{aligned}$$

This and a Pythagoras theorem conclude the proof (for details see the end of the proof for the pressure-robust case). □

Proof of (B). Subtracting the continuous problem (2) from the pressure-robust discrete problem (14) for $\nu = 0$ and $s \in (0,t)$ and inserting $\mathbf{f}(s) = \mathbf{u}_t(s) + \nabla p(s)$ gives

$$\frac{d}{dt}(\mathbf{u}(s) - \Pi\mathbf{u}_h(s), \Pi\mathbf{v}_h) = 0$$

for any (time-independent) test function $\mathbf{v}_h \in \boldsymbol{X}_{h,\text{div}}$. Integration over $(0,t)$ gives

$$(\mathbf{u}(t) - \Pi\mathbf{u}_h(t), \Pi\mathbf{v}_h) = (\mathbf{u}(0) - \Pi\mathbf{u}_h(0), \Pi\mathbf{v}_h) \leq \|\mathbf{u}(0) - \Pi\mathbf{u}_h(0)\|_{L^2(\Omega)} \|\Pi\mathbf{v}_h\|_{L^2(\Omega)}.$$

Moreover, for the best approximation $\Pi\mathbf{w}_h$ of $\mathbf{u}(t)$ in $\Pi\boldsymbol{X}_{h,\text{div}}$ with $\mathbf{w}_h - \mathbf{u}_h = 0$ along $\partial\Omega$, it holds

$$(\Pi\mathbf{w}_h - \mathbf{u}(t), \Pi\mathbf{v}_h) = 0.$$

Hence, testing with the test function $\mathbf{v}_h := \mathbf{u}_h(t) - \mathbf{w}_h \in \boldsymbol{X}_{h,\text{div}}$ gives

$$\begin{aligned}\|\Pi\mathbf{v}_h\|^2_{L^2(\Omega)} = \|\Pi\mathbf{w}_h - \Pi\mathbf{u}_h(t)\|^2_{L^2(\Omega)} &= (\Pi\mathbf{w}_h - \mathbf{u}(t), \Pi\mathbf{v}_h) + (\mathbf{u}(t) - \Pi\mathbf{u}_h(t), \Pi\mathbf{v}_h) \\ &\leq \|\mathbf{u}(0) - \Pi\mathbf{u}_h(0)\|_{L^2(\Omega)} \|\Pi\mathbf{v}_h\|_{L^2(\Omega)}.\end{aligned}$$

Division by $\|\Pi\mathbf{v}_h\|_{L^2(\Omega)}$ shows $\|\Pi\mathbf{w}_h - \Pi\mathbf{u}_h(t)\|_{L^2(\Omega)} \leq \|\mathbf{u}(0) - \Pi\mathbf{u}_h(0)\|_{L^2(\Omega)}$ and the Pythagoras theorem (note that $(\mathbf{u}(t) - \Pi\mathbf{w}_h, \Pi\mathbf{w}_h - \Pi\mathbf{u}_h(t)) = 0$)

$$\|\mathbf{u}(t) - \Pi\mathbf{u}_h(t)\|^2_{L^2(\Omega)} = \|\mathbf{u}(t) - \Pi\mathbf{w}_h\|^2_{L^2(\Omega)} + \|\Pi\mathbf{w}_h - \Pi\mathbf{u}_h(t)\|^2_{L^2(\Omega)}$$

concludes the proof for the pressure-robust discretization. □

Remark 4.2. *To illustrate this result we perform a short numerical experiment with the prescribed exact solution* $\mathbf{u} \equiv 0$ *and (time-dependent) pressure*

$$p_\gamma(t,x,y) = (1 + \gamma\cos(10\pi t))(\sin(\pi x)\cos(\pi y)) \text{ with } \gamma \in \{0,1,2\} \tag{16}$$

and the right-hand side $\mathbf{f}(t) := \nabla p_\gamma(t)$. *To approach the time-continuous case as close as possible we use a backward Euler time discretization with time-step* $\tau = 10^{-4}$ *and* $\nu = 0$ *in the time interval* $(0,1)$. *Figure 1 shows the* L^2*-error of the classical Bernardi–Raugel finite element method for all three choices of* γ *(the pressure-robust Bernardi–Raugel discretization has zero error in this case as predicted by Theorem 4.1 and is not plotted). The error of the classical method grows linearly in time for* $\gamma = 0$ *and also for* $\gamma = 1$ *or* $\gamma = 2$ *(besides some oscillations caused by the oscillating part of the pressure). The case* $\gamma = 2$ *shows that if the pressure changes directions it can lead to a reduction of the error that was accumulated before. All cases arrive at the same error, since the total integral of the pressure over the interval* $(0,1)$ *is the same for all choices of* γ. *Altogether this little example shows that the error estimate in Theorem 4.1 is sharp.*

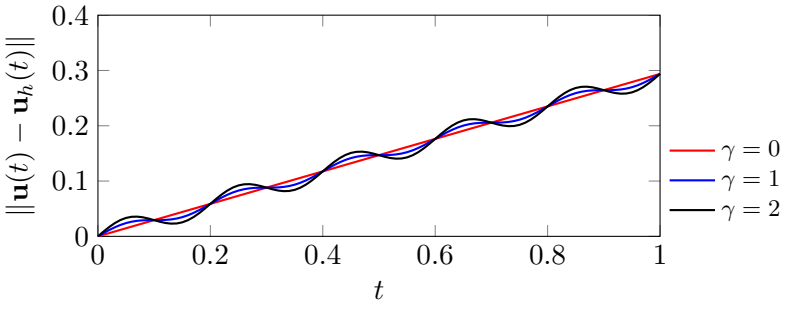

Figure 1: L^2 error of the classical Bernardi–Raugel finite element method for the limit case example with $\mathbf{u} \equiv 0$ and pressure (16) for $\gamma \in \{0,1,2\}$.

Remark 4.3. *The convergence orders in the limit case are optimal on shape-regular meshes, as argued in Remarks 3.7 and 3.8.*

5 Time discretization

In this section, the semi-discrete problems (9) and (14) are further discretized in time using the classical θ-scheme to obtain the fully discrete problem. To this end, consider a non-negative integer N and a uniform time step length $\tau := T/N$ where T is the final time. In the following $(\mathbf{u}_h^n, p_h^n)$ stands for an approximation of $(\mathbf{u}(t^n), p(t^n))$ with $t^n := n\tau$ for $1 \leq n \leq N$. Note, that the following a priori error analysis extends to non-uniform time-step sizes in a straight-forward way, but is avoided here to concentrate on the pressure-robustness.

5.1 Time stepping with the θ–scheme

The fully discrete classical mixed FEM discretized in time using the classical θ-scheme with $\theta \in [1/2, 1]$ reads: For given $\mathbf{u}_h^0$ a suitable approximation of the initial velocity $\mathbf{u}_0$ in $\mathbf{V}_h$, find $(\mathbf{u}_h^n, p_h^n) \in \mathbf{V}_h \times Q_h$ with $1 \leq n \leq N$, that satisfy

$$\left\{ \begin{array}{rl} (\mathbf{u}_{h,\tau}^n, \mathbf{v}_h) + \nu(\nabla \mathbf{u}_h^{n-\theta}, \nabla \mathbf{v}_h) - (p_h^n, \nabla \cdot \mathbf{v}_h) = (\mathbf{f}^{n-\theta}, \mathbf{v}_h) & \forall \mathbf{v}_h \in \mathbf{V}_h, \\ (q_h, \nabla \cdot \mathbf{u}_h^{n-\theta}) = 0 & \forall q_h \in Q_h \end{array} \right. \tag{17}$$

where $\mathbf{u}_{h,\tau}^n := (\mathbf{u}_h^n - \mathbf{u}_h^{n-1})/\tau$, $\mathbf{u}_h^{n-\theta} := \theta \mathbf{u}_h^n + (1-\theta)\mathbf{u}_h^{n-1}$ and $\mathbf{f}^{n-\theta} := \mathbf{f}(t^{n-\theta})$ with $t^{n-\theta} := \theta t^n + (1-\theta) t^{n-1}$. For $\theta = 1$ this yields the backward Euler scheme and for $\theta = 0.5$ the Crank-Nicolson scheme.

Similarly, the classical θ-scheme applied to the pressure-robust mixed FEM (14) reads as follows: For given $\mathbf{u}_h^0$ and $1 \leq n \leq N$, find $(\mathbf{u}_h^n, p_h^n) \in \mathbf{V}_h \times Q_h$ such that

$$\left\{ \begin{array}{rl} (\Pi \mathbf{u}_{h,\tau}^n, \Pi \mathbf{v}_h) + \nu(\nabla \mathbf{u}_h^{n-\theta}, \nabla \mathbf{v}_h) - (p_h^n, \nabla \cdot \mathbf{v}_h) = (\mathbf{f}^{n-\theta}, \Pi \mathbf{v}_h) & \forall \mathbf{v}_h \in \mathbf{V}_h, \\ (q_h, \nabla \cdot \mathbf{u}_h^{n-\theta}) = 0 & \forall q_h \in Q_h. \end{array} \right. \tag{18}$$

In the analysis of the fully discrete schemes, the following discrete version of the Gronwall's inequality will be used, see [27, 24].

Lemma 5.1. *Let τ, B and a_j, b_j, c_j, γ_j, for $j \geq 1$, be non-negative numbers such that*

$$a_n + \sum_{j=1}^{n} b_j \leq B + \tau \sum_{j=1}^{n} c_j + \tau \sum_{j=1}^{n} \gamma_j a_j$$

holds. If $\tau\gamma_j < 1$ for all $j = 1, \ldots, n$, then

$$a_n + \sum_{j=1}^{n} b_j \leq \exp\left(\tau \sum_{j=1}^{n} \frac{\gamma_j}{1 - \tau\gamma_j} \right) \left(B + \tau \sum_{j=1}^{n} c_j \right).$$

Furthermore, the following short form of the norms will be used for a fixed time step index n:

$$\|\mathbf{v}\|_{0,\tau}^2 := \sum_{j=1}^{n} \tau \|\mathbf{v}^j\|_{L^2(\Omega)}^2, \quad \|\mathbf{v}\|_{\theta,\tau}^2 := \sum_{j=1}^{n} \tau \|\mathbf{v}^{j-\theta}\|_{L^2(\Omega)}^2, \quad \|\mathbf{v}\|_{\theta,\tau,\boldsymbol{X}_{h,\mathrm{div}}^\star}^2 := \sum_{j=1}^{n} \tau \|\mathbf{v}^{j-\theta}\|_{\boldsymbol{X}_{h,\mathrm{div}}^\star}^2.$$

In cases where the summation indices change, the complete form of the norms will be used. The next theorem states the stability of the θ-schemes (17) and (18).

Theorem 5.2 (Stability of the θ-schemes (17) and (18))**.** *Let $\mathbf{u}_h^0$ be a given approximation of the initial velocity $\mathbf{u}_0$ in $\mathbf{V}_h$. For the solution $(\mathbf{u}_h^n, p_h^n)$ of the fully discrete scheme* (17)*, the following estimate holds for $1 \leq n \leq N$ with $C_{\mathsf{G}} = \exp\left(T(T-\tau)^{-1}\right)$*

$$\begin{aligned}&\frac{1}{2}\left\|\mathbf{u}_h^n\right\|_{L^2(\Omega)}^2 + \frac{\nu}{2}\left\|\nabla \mathbf{u}_h\right\|_{\theta,\tau}^2 \\ &\quad\leq \min\left\{\left(\frac{1}{2}\|\mathbf{u}_h^0\|_{L^2(\Omega)}^2 + \frac{1}{2\nu}\|\mathbb{P}_h(\mathbf{f})\|_{\theta,\tau,\boldsymbol{X}_{h,\mathsf{div}}^\star}^2\right), C_{\mathsf{G}}\left(\frac{1}{2}\|\mathbf{u}_h^0\|_{L^2(\Omega)}^2 + T\|\mathbb{P}_h(\mathbf{f})\|_{\theta,\tau}^2\right)\right\} \quad (19)\end{aligned}$$

and for the solution $(\mathbf{u}_h^n, p_h^n)$ of the fully discrete scheme (18) *one gets*

$$\begin{aligned}\frac{1}{2}\left\|\Pi\mathbf{u}_h^n\right\|_{L^2(\Omega)}^2 + \frac{\nu}{2}\left\|\nabla \mathbf{u}_h\right\|_{\theta,\tau}^2 \leq \min\Bigg\{&\left(\frac{1}{2}\left\|\Pi\mathbf{u}_h^0\right\|_{L^2(\Omega)}^2 + \frac{1}{2\nu}\left\|\mathbb{P}_h^\star(\mathbf{f})\circ\Pi\right\|_{\theta,\tau,\boldsymbol{X}_{h,\mathsf{div}}^\star}^2\right), \\ &C_{\mathsf{G}}\left(\frac{1}{2}\|\Pi\mathbf{u}_h^0\|_{L^2(\Omega)}^2 + T\left\|\mathbb{P}_h^\star(\mathbf{f})\right\|_{\theta,\tau}^2\right)\Bigg\}. \quad (20)\end{aligned}$$

Proof. The solution $\mathbf{u}_h^j \in \boldsymbol{X}_{h,\mathsf{div}}$ of (17) for time step $j \in \{1,\dots,n\}$ satisfies

$$\tau(\mathbf{u}_{h,\tau}^j, \mathbf{v}_h) + \nu\tau(\nabla \mathbf{u}_h^{j-\theta}, \nabla \mathbf{v}_h) = \tau(\mathbf{f}^{j-\theta}, \mathbf{v}_h) = \tau(\mathbb{P}_h(\mathbf{f}^{j-\theta}), \mathbf{v}_h) \quad \forall \mathbf{v}_h \in \boldsymbol{X}_{h,\mathsf{div}}. \quad (21)$$

For $\mathbf{v}_h = \mathbf{u}_h^{j-\theta}$, elementary calculations show

$$\begin{aligned}&\tau(\mathbf{u}_{h,\tau}^j, \mathbf{v}_h) = (\mathbf{u}_h^j - \mathbf{u}_h^{j-1}, \theta\mathbf{u}_h^j + (1-\theta)\mathbf{u}_h^{j-1}) \\ &= \frac{1}{2}\left(\left\|\mathbf{u}_h^j\right\|_{L^2(\Omega)}^2 - \left\|\mathbf{u}_h^{j-1}\right\|_{L^2(\Omega)}^2\right) + \frac{2\theta-1}{2}\left\|\mathbf{u}_h^j - \mathbf{u}_h^{j-1}\right\|_{L^2(\Omega)}^2 \geq \frac{1}{2}\left\|\mathbf{u}_h^j\right\|_{L^2(\Omega)}^2 - \frac{1}{2}\left\|\mathbf{u}_h^{j-1}\right\|_{L^2(\Omega)}^2.\end{aligned}$$

This and Cauchy–Schwarz and Young inequalities applied to the right-hand side of (21) lead to

$$\begin{aligned}&\frac{1}{2}\left\|\mathbf{u}_h^j\right\|_{L^2(\Omega)}^2 - \frac{1}{2}\left\|\mathbf{u}_h^{j-1}\right\|_{L^2(\Omega)}^2 + \nu\tau\left\|\nabla \mathbf{u}_h^{j-\theta}\right\|_{L^2(\Omega)}^2 \\ &\leq \min\left\{\frac{\tau}{2\nu}\|\mathbb{P}_h(\mathbf{f}^{j-\theta})\|_{\boldsymbol{X}_{h,\mathsf{div}}^\star}^2 + \frac{\nu\tau}{2}\|\nabla \mathbf{u}_h^{j-\theta}\|_{L^2(\Omega)}^2, T\tau\left\|\mathbb{P}_h(\mathbf{f}^{j-\theta})\right\|_{L^2(\Omega)}^2 + \frac{\tau}{4T}\|\mathbf{u}_h^{j-\theta}\|_{L^2(\Omega)}^2\right\}.\end{aligned}$$

Summation over $j = 1,\dots,n$ and $\|\mathbf{u}_h\|_{\theta,\tau}^2 \leq 2\sum_{j=0}^{n}\tau\|\mathbf{u}_h^j\|_{L^2(\Omega)}^2 = \|\mathbf{u}_h\|_{0,\tau}^2 + \frac{\tau}{2T}\|\mathbf{u}_h^0\|_{L^2(\Omega)}^2$ gives

$$\begin{aligned}\frac{1}{2}\left\|\mathbf{u}_h^n\right\|_{L^2(\Omega)}^2 + \nu\left\|\nabla \mathbf{u}_h\right\|_{\theta,\tau}^2 \leq \frac{1}{2}\|\mathbf{u}_h^0\|_{L^2(\Omega)}^2 + \min\Bigg\{&\frac{1}{2\nu}\|\mathbb{P}_h(\mathbf{f})\|_{\theta,\tau,\boldsymbol{X}_{h,\mathsf{div}}^\star}^2 + \frac{\nu}{2}\|\nabla \mathbf{u}_h^{n-\theta}\|_{\theta,\tau}^2, \\ &T\left\|\mathbb{P}_h(\mathbf{f})\right\|_{\theta,\tau}^2 + \frac{1}{2T}\|\mathbf{u}_h\|_{0,\tau}^2 + \frac{\tau}{2T}\|\mathbf{u}_h^0\|_{L^2(\Omega)}^2\Bigg\}.\end{aligned}$$

The first statement of the theorem now follows by absorbing the $\|\nabla \mathbf{u}_h\|_{\theta,\tau}^2$-norm in the min case on the right-hand side to the left-hand side, and by applying Lemma 5.1 to the second min case on the right-hand side, taking $\gamma_j = 1/T$ such that $\tau\gamma_j = \tau/T < 1$.

Similarly, the solution $\mathbf{u}_h^j \in \boldsymbol{X}_{h,\mathsf{div}}$ of (18) satisfies

$$\tau\left(\Pi\mathbf{u}_{h,\tau}^j, \Pi\mathbf{v}_h\right) + \nu\tau\left(\nabla \mathbf{u}_h^{j-\theta}, \nabla \mathbf{v}_h\right) = \tau\left(\mathbf{f}^{j-\theta}, \Pi\mathbf{v}_h\right) = \tau\left(\mathbb{P}_h^\star(\mathbf{f}^{j-\theta}), \Pi\mathbf{v}_h\right) \quad \forall \mathbf{v}_h \in \boldsymbol{X}_{h,\mathsf{div}}.$$

Setting $\mathbf{v}_h = \mathbf{u}_h^{j-\theta}$, using the same algebraic inequality as in the previous estimate, and the Cauchy–Schwarz inequality gives

$$\begin{aligned}
&\frac{1}{2}\left\|\Pi\mathbf{u}_h^j\right\|^2_{L^2(\Omega)} - \frac{1}{2}\left\|\Pi\mathbf{u}_h^{j-1}\right\|^2_{L^2(\Omega)} + \nu\tau\left\|\nabla\mathbf{u}_h^{j-\theta}\right\|_{L^2(\Omega)} \\
&\leq \tau\min\left\{\nu^{-1/2}\left\|\mathbb{P}_h^\star(\mathbf{f}^{j-\theta})\circ\Pi\right\|_{\boldsymbol{X}_{h,\mathsf{div}}^\star}\nu^{1/2}\left\|\nabla\mathbf{u}_h^{j-\theta}\right\|_{L^2(\Omega)}, \left\|\mathbb{P}_h^\star(\mathbf{f}^{j-\theta})\right\|_{L^2(\Omega)}\left\|\Pi\mathbf{u}_h^{j-\theta}\right\|_{L^2(\Omega)}\right\}.
\end{aligned}$$

The rest of the proof is identically to the classical case. □

5.2 Error estimates of the fully discrete schemes

In this section the a priori error estimates for the fully discrete classical scheme (17) as well as for the novel pressure-robust scheme (18) are derived.

The next theorem states the convergence results of the fully discrete θ-schemes of the classical and the pressure-robust mixed finite element methods.

Theorem 5.3 (Error estimates of θ-schemes)**.** *Let* $(\mathbf{u}(t^n), p(t^n))$ *be the solution of* (2) *and assume* $\mathbf{u}_t, \mathbf{u}_{tt}, \mathbf{u}_{ttt} \in L^2(0,t;L^2(\Omega))$.

(A) For the solution $(\mathbf{u}_h^n, p_h^n)$ *of the fully discrete classical* θ*-scheme* (17) *for* $n = 1,\dots,N \geq 1$*, it holds, for arbitrary* $\mathbf{w}_h \in L^2(0,t;\boldsymbol{X}_{h,\mathsf{div}})$ *with* $\mathbf{u}_h^0 = \mathbf{w}_h^0$*,*

$$\begin{aligned}
\|\mathbf{u}(t^n)-\mathbf{u}_h^n\|^2_{L^2(\Omega)} + \nu\|\nabla(\mathbf{u}-\mathbf{u}_h)\|^2_{\theta,\tau} &\leq 2\|\mathbf{u}(t^n)-\mathbf{w}_h^n\|^2_{L^2(\Omega)} + 2\nu\|\nabla(\mathbf{u}-\mathbf{w}_h)\|^2_{\theta,\tau} \\
&+ C\min\left\{\left(\frac{1}{\nu}\left\|\mathbb{P}_h(\mathbf{u}_t-\mathbf{w}_{h,t}+\nabla p)\right\|^2_{\theta,\tau,\boldsymbol{X}_{h,\mathsf{div}}^\star} + \frac{\tau^2|2\theta-1|}{\nu}\left\|\mathbb{P}_h(\mathbf{w}_{h,tt})\right\|^2_{\theta,\tau,\boldsymbol{X}_{h,\mathsf{div}}^\star}\right.\right. \\
&\qquad \left. + \frac{\tau^4}{\nu}\left\|\mathbb{P}_h(\mathbf{w}_{h,ttt})\right\|^2_{L^2(0,t;\boldsymbol{X}_{h,\mathsf{div}}^\star)} + \nu\|\nabla(\mathbf{u}-\mathbf{w}_h)\|^2_{\theta,\tau}\right), \\
&\quad C_{\mathsf{G}}\left(T\left\|\mathbb{P}_h(\mathbf{u}_t-\mathbf{w}_{h,t}+\nabla p)\right\|^2_{\theta,\tau} + \tau^2 T|2\theta-1|\left\|\mathbb{P}_h(\mathbf{w}_{h,tt})\right\|^2_{\theta,\tau}\right. \\
&\qquad \left.\left. + \tau^4 T\left\|\mathbb{P}_h(\mathbf{w}_{h,ttt})\right\|^2_{L^2(0,t;L^2)} + \nu\|\nabla(\mathbf{u}-\mathbf{w}_h)\|^2_{\theta,\tau}\right)\right\}.
\end{aligned}$$

(B) Similarly, for the solution $(\mathbf{u}_h^n, p_h^n)$ *of the fully discrete pressure-robust* θ*-scheme* (18) *for* $n = 1,\dots,N \geq 1$*, it holds for arbitrary* $\mathbf{w}_h \in L^2(0,t;\boldsymbol{X}_{h,\mathsf{div}})$ *with* $\mathbf{u}_h^0 = \mathbf{w}_h^0$*,*

$$\begin{aligned}
\|\mathbf{u}(t^n)-\Pi\mathbf{u}_h^n\|^2_{L^2(\Omega)} + \nu\|\nabla(\mathbf{u}-\mathbf{u}_h)\|^2_{\theta,\tau} &\leq 2\|\mathbf{u}(t^n)-\Pi\mathbf{w}_h^n\|^2_{L^2(\Omega)} + 2\nu\|\nabla(\mathbf{u}-\mathbf{w}_h)\|^2_{\theta,\tau} \\
+C\min\left\{\left(\nu\|\nabla(\mathbf{u}-\mathbf{w}_h)\|^2_{\theta,\tau} + \nu\left\|\Delta\mathbf{u}\circ(1-\Pi)\right\|^2_{\theta,\tau,\boldsymbol{X}_{h,\mathsf{div}}^\star} + \frac{1}{\nu}\left\|\mathbb{P}_h^\star(\mathbf{u}_t-\Pi\mathbf{w}_{h,t})\circ\Pi\right\|^2_{\theta,\tau,\boldsymbol{X}_{h,\mathsf{div}}^\star}\right.\right. \\
\qquad + \frac{\tau^2|2\theta-1|}{\nu}\left\|\mathbb{P}_h^\star(\Pi\mathbf{w}_{h,tt})\circ\Pi\right\|^2_{\theta,\tau,\boldsymbol{X}_{h,\mathsf{div}}^\star} + \frac{\tau^4}{\nu}\left\|\mathbb{P}_h^\star(\Pi\mathbf{w}_{h,ttt})\circ\Pi\right\|^2_{L^2(0,t;\boldsymbol{X}_{h,\mathsf{div}}^\star)}\Big), \\
C_{\mathsf{G}}\Big(\nu\|\nabla(\mathbf{u}-\mathbf{w}_h)\|^2_{\theta,\tau} + \nu\left\|\Delta\mathbf{u}\circ(1-\Pi)\right\|^2_{\theta,\tau,\boldsymbol{X}_{h,\mathsf{div}}^\star} + T\left\|\mathbb{P}_h^\star(\mathbf{u}_t-\Pi\mathbf{w}_{h,t})\right\|^2_{\theta,\tau} \\
\left.\left. + \tau^2 T|2\theta-1|\left\|\mathbb{P}_h^\star(\Pi\mathbf{w}_{h,tt})\right\|^2_{\theta,\tau} + \tau^4 T\left\|\mathbb{P}_h^\star(\Pi\mathbf{w}_{h,ttt})\right\|^2_{L^2(0,t;L^2)}\Big)\right\}.
\end{aligned}$$

Here $C_{\mathsf{G}} = \exp\left(T(T-\tau)^{-1}\right)$ *and* C *is a constant independent of* h, τ, *and* ν.

Proof. We just prove the novel estimate (B) for the pressure-robust scheme. The proof of the classical estimate (A) follows analogously.

The error equation for the fully discrete θ-scheme with pressure-robust mixed FEM is obtained by subtracting (2) from (18) and using $\mathbf{f} = \mathbf{u}_t - \nu\Delta\mathbf{u} + \nabla p$, that is

$$\begin{aligned}(\Pi\mathbf{e}_{h,\tau}^n, \Pi\mathbf{v}_h) + \nu(\nabla\mathbf{e}_h^{n-\theta}, \nabla\mathbf{v}_h) \\ = \left(T_{\mathsf{tr}}^{\mathsf{pr}}, \Pi\mathbf{v}_h\right) + \nu(\nabla(\mathbf{u}(t^{n-\theta}) - \mathbf{w}_h^{n-\theta}), \nabla\mathbf{v}_h) - \nu(\Delta\mathbf{u}(t^{n-\theta}), \mathbf{v}_h - \Pi\mathbf{v}_h) \quad (22)\end{aligned}$$

where $T_{\mathsf{tr}}^{\mathsf{pr}} := \mathbf{u}_t(t^{n-\theta}) - \tau^{-1}(\Pi\mathbf{w}_h^n - \Pi\mathbf{w}_h^{n-1})$. The last term on the right-hand sides of (22) is bounded by the consistency error (11) and the Young's inequality

$$\begin{aligned}\nu(\Delta\mathbf{u}(t^{n-\theta}), \mathbf{v}_h - \Pi\mathbf{v}_h) &\le \nu\|\Delta\mathbf{u}(t^{n-\theta}) \circ (1-\Pi)\|_{\boldsymbol{X}_{h,\mathsf{div}}^\star}\|\nabla\mathbf{v}_h\|_{L^2(\Omega)} \\ &\le \nu\|\Delta\mathbf{u}(t^{n-\theta}) \circ (1-\Pi)\|_{\boldsymbol{X}_{h,\mathsf{div}}^\star}^2 + \frac{\nu}{4}\|\nabla\mathbf{v}_h\|_{L^2(\Omega)}^2.\end{aligned}$$

The first two terms on the right hand sides of (22) are estimated in a similar fashion by using the Cauchy–Schwarz and Young's inequalities. Using similar steps as in the stability estimate (20), one gets

$$\begin{aligned}&\|\Pi\mathbf{e}_h^n\|_{L^2(\Omega)}^2 + \nu\|\nabla\mathbf{e}_h\|_{\theta,\tau}^2 \\ &\le \min\left\{ \left(\frac{4}{\nu}\left\|\mathbb{P}_h^\star(T_{\mathsf{tr}}^{\mathsf{pr}}) \circ \Pi\right\|_{\theta,\tau,\boldsymbol{X}_{h,\mathsf{div}}^\star}^2 + \nu\left\|\Delta\mathbf{u} \circ (1-\Pi)\right\|_{\theta,\tau,\boldsymbol{X}_{h,\mathsf{div}}^\star}^2 + 4\nu\|\nabla(\mathbf{u}-\mathbf{w}_h)\|_{\theta,\tau}^2\right), \right. \\ &\qquad \left. C_{\mathsf{G}}\left(2T\left\|\mathbb{P}_h^\star(T_{\mathsf{tr}}^{\mathsf{pr}})\right\|_{\theta,\tau}^2 + \nu\left\|\Delta\mathbf{u} \circ (1-\Pi)\right\|_{\theta,\tau,\boldsymbol{X}_{h,\mathsf{div}}^\star}^2 + 2\nu\|\nabla(\mathbf{u}-\mathbf{w}_h)\|_{\theta,\tau}^2\right)\right\} \quad (23)\end{aligned}$$

where in addition $\mathbf{e}_h^0 = 0$ was exploited. It remains to get the bounds for the error terms $T_{\mathsf{tr}}^{\mathsf{pr}}$. To achieve this, the application of the triangle inequality gives

$$\begin{aligned}\left\|\mathbb{P}_h \star (T_{\mathsf{tr}}^{\mathsf{pr}})\right\|_{\theta,\tau}^2 &= \sum_{j=1}^n \tau\left\|\mathbb{P}_h^\star\left(\mathbf{u}_t(t^{j-\theta}) - \tau^{-1}\left(\Pi\mathbf{w}_h^n - \Pi\mathbf{w}_h^{n-1}\right)\right)\right\|_{L^2(\Omega)}^2 \\ &\le 2\left[\left\|\mathbb{P}_h^\star\left(\mathbf{u}_t - \Pi\mathbf{w}_t\right)\right\|_{\theta,\tau}^2 + \sum_{j=1}^n \tau\left\|\mathbb{P}_h^\star\left(\Pi\mathbf{w}_{h,t}(t^{j-\theta}) - \tau^{-1}\left(\Pi\mathbf{w}_h^j - \Pi\mathbf{w}_h^{j-1}\right)\right)\right\|_{L^2(\Omega)}^2\right].\end{aligned}$$

The second term can be treated in a standard way, see e.g. [40], using a Taylor series expansion with integral remainder term for $\theta \in [1/2, 1]$, which yields

$$\begin{aligned}\Pi\mathbf{w}_{h,t}(t^{j-\theta}) - \frac{\Pi\mathbf{w}_h^j - \Pi\mathbf{w}_h^{j-1}}{\tau} = \\ \frac{\tau}{2}(2\theta-1)\Pi\mathbf{w}_{h,tt}(t^{j-\theta}) - \frac{1}{2\tau}\left[\int_{t^{j-1}}^{t^{j-\theta}}(t-t^{j-1})^2\Pi\mathbf{w}_{h,ttt} + \int_{t^{j-\theta}}^{t^j}(t-t^j)^2\Pi\mathbf{w}_{h,ttt}\right].\end{aligned}$$

Then, using the Cauchy–Schwarz inequality and Fubini theorem, one gets

$$\begin{aligned}
&\sum_{j=1}^{n} \tau \left\| \mathbb{P}_h^\star \left(\Pi \mathbf{w}_{h,t}(t^{j-\theta}) - \tau^{-1}(\Pi \mathbf{w}_h^j - \Pi \mathbf{w}_h^{j-1}) \right) \right\|_{L^2(\Omega)}^2 \\
&\quad \le C\tau^2 |2\theta - 1| \sum_{j=1}^{n} \tau \left\| \mathbb{P}_h^\star (\Pi \mathbf{w}_{h,tt}(t^{j-\theta})) \right\|_{L^2(\Omega)}^2 \\
&\qquad + \frac{C}{\tau} \sum_{j=1}^{n} \int_{t^{j-1}}^{t^{j-\theta}} (t - t^{j-1})^4 \int_{t^{j-1}}^{t^{j-\theta}} \|\mathbb{P}_h^\star (\Pi \mathbf{w}_{h,ttt})\|_{L^2(\Omega)}^2 \\
&\qquad + \frac{C}{\tau} \sum_{j=1}^{n} \int_{t^{j-\theta}}^{t^{j}} (t - t^{j})^4 \int_{t^{j-\theta}}^{t^{j}} \|\mathbb{P}_h^\star (\Pi \mathbf{w}_{h,ttt})\|_{L^2(\Omega)}^2 \\
&\quad \le C\tau^2 |2\theta - 1| \, \|\mathbb{P}_h^\star (\Pi \mathbf{w}_{h,tt})\|_{\theta,\tau}^2 + C\tau^4 \, \|\mathbb{P}_h^\star (\Pi \mathbf{w}_{h,ttt})\|_{L^2(0,t;L^2)}^2 .
\end{aligned}$$

Collecting the above estimate, one gets

$$\begin{aligned}
\left\| \mathbb{P}_h^\star (T_{\mathsf{tr}}^{\mathsf{pr}}) \right\|_{\theta,\tau}^2 \le C \Big[& \|\mathbb{P}_h^\star (\mathbf{u}_t - \Pi \mathbf{w}_{h,t})\|_{\theta,\tau}^2 \\
& + \tau^2 |2\theta - 1| \, \|\mathbb{P}_h^\star (\Pi \mathbf{w}_{h,tt})\|_{\theta,\tau}^2 + \tau^4 \, \|\mathbb{P}_h^\star (\Pi \mathbf{w}_{h,ttt})\|_{L^2(0,t;L^2)}^2 \Big].
\end{aligned}$$

Similar arguments can be used to bound the term $\|T_{\mathsf{tr}}^{\mathsf{pr}}\|_{\tau,\theta,\boldsymbol{X}_{h,\mathsf{div}}^\star}$, which leads to

$$\begin{aligned}
\left\| \mathbb{P}_h^\star (T_{\mathsf{tr}}^{\mathsf{pr}}) \circ \Pi \right\|_{\theta,\tau,\boldsymbol{X}_{h,\mathsf{div}}^\star}^2 \le C \Big[& \|\mathbb{P}_h^\star (\mathbf{u}_t - \Pi \mathbf{w}_{h,t}) \circ \Pi\|_{\theta,\tau,\boldsymbol{X}_{h,\mathsf{div}}^\star}^2 + \tau^2 |2\theta - 1| \; \|\mathbb{P}_h^\star (\Pi \mathbf{w}_{h,tt}) \circ \Pi\|_{\theta,\tau,\boldsymbol{X}_{h,\mathsf{div}}^\star}^2 \\
& + \tau^4 \, \|\mathbb{P}_h^\star (\Pi \mathbf{w}_{h,ttt}) \circ \Pi\|_{L^2(0,t;\boldsymbol{X}_{h,\mathsf{div}}^\star)}^2 \Big].
\end{aligned}$$

By inserting this expression in (23) and using $\mathbf{e}_h^0 = 0$ leads to the following error bound

$$\begin{aligned}
&\|\Pi \mathbf{e}_h^n\|_{L^2(\Omega)}^2 + \nu \|\nabla \mathbf{e}_h\|_{\theta,\tau}^2 \\
&\le C \min \Bigg\{ \Bigg(\nu \|\nabla(\mathbf{u} - \mathbf{w}_h)\|_{\theta,\tau}^2 + \nu \, \|\Delta \mathbf{u} \circ (1 - \Pi)\|_{\theta,\tau,\boldsymbol{X}_{h,\mathsf{div}}^\star}^2 + \frac{1}{\nu} \, \|\mathbb{P}_h^\star (\mathbf{u}_t - \Pi \mathbf{w}_{h,t}) \circ \Pi\|_{\theta,\tau,\boldsymbol{X}_{h,\mathsf{div}}^\star}^2 \\
&\qquad + \frac{\tau^2 |2\theta - 1|}{\nu} \; \|\mathbb{P}_h^\star (\Pi \mathbf{w}_{h,tt}) \circ \Pi\|_{\theta,\tau,\boldsymbol{X}_{h,\mathsf{div}}^\star}^2 + \frac{\tau^4}{\nu} \, \|\mathbb{P}_h^\star (\Pi \mathbf{w}_{h,ttt}) \circ \Pi\|_{L^2(0,t;\boldsymbol{X}_{h,\mathsf{div}}^\star)}^2 \Bigg), \\
&\quad C_{\mathsf{G}} \Bigg(\nu \|\nabla(\mathbf{u} - \mathbf{w}_h)\|_{\theta,\tau}^2 + \nu \, \|\Delta \mathbf{u} \circ (1 - \Pi)\|_{\theta,\tau,\boldsymbol{X}_{h,\mathsf{div}}^\star}^2 + T \, \|\mathbb{P}_h^\star (\mathbf{u}_t - \Pi \mathbf{w}_{h,t})\|_{\theta,\tau}^2 \\
&\qquad + \tau^2 T |2\theta - 1| \; \|\mathbb{P}_h^\star (\Pi \mathbf{w}_{h,tt})\|_{\theta,\tau}^2 + \tau^4 T \, \|\mathbb{P}_h^\star (\Pi \mathbf{w}_{h,ttt})\|_{L^2(0,t;L^2)}^2 \Bigg) \Bigg\}.
\end{aligned}$$

This estimate and the application of the triangle inequality

$$\begin{aligned}
&\|\mathbf{u}(t^n) - \Pi \mathbf{u}_h^n\|_{L^2(\Omega)}^2 + \nu \|\nabla(\mathbf{u}(t^n) - \mathbf{u}_h^n)\|_{L^2(\Omega)}^2 \\
&\le 2 \left(\|\mathbf{u}(t^n) - \Pi \mathbf{w}_h^n\|_{L^2(\Omega)}^2 + \nu \|\nabla(\mathbf{u}(t^n) - \mathbf{w}_h^n)\|_{L^2(\Omega)}^2 \right) + 2 \left(\|\Pi \mathbf{e}_h^n\|_{L^2(\Omega)}^2 + \nu \|\nabla \mathbf{e}_h^n)\|_{L^2(\Omega)}^2 \right)
\end{aligned}$$

concludes the proof of (B). □

Remark 5.4. *As in the time-continuous case, it is possible to achieve $\mathbb{P}_h(\mathbf{u}_t - \mathbf{w}_{h,t}) = 0$ in case (A) or $\mathbb{P}_h^\star(\mathbf{u}_t - \Pi \mathbf{w}_{h,t}) = 0$ in case (B) by choosing proper best approximations, i.e. $\mathbf{w}_h = \mathbb{P}_h(\mathbf{u})$ or $\Pi \mathbf{w}_h = \mathbb{P}_h^\star(\mathbf{u})$, respectively, compare with Theorems 3.1.(B) and 3.6.(B). Opposite to the time-continuous case the terms with the higher time derivatives of $\mathbf{w}_h$ remain.*

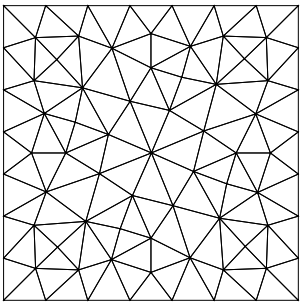

Figure 2: Initial mesh (level = 0) for the numerical simulations.

6 Numerical studies

This section studies two numerical examples to support the theoretical findings by numerical evidence. Both examples employ uniform refinements of the unstructured initial mesh depicted in Fig. 2 of the unit square $\Omega := (0,1)^2$.

To compare the classical and the modified finite element methods, the problem is solved on the time interval $(0,1]$. The viscosity parameter ν and the time step length τ are varied to show their influence on the cumulative $L^2(\Omega)$ gradient error of the velocity defined by

$$\|\nabla(\mathbf{u}-\mathbf{u}_h)\|_{\tau,h}^2 := \sum_{n=1}^{N} \frac{\tau}{2}\left(\|\nabla(\mathbf{u}(t_{n-1})-\mathbf{u}_h^{n-1})\|_{L^2(\Omega)}^2 + \|\nabla(\mathbf{u}(t_n)-\mathbf{u}_h^{n})\|_{L^2(\Omega)}^2\right).$$

6.1 Analytic example with zero boundary data

This example studies the velocity and pressure

$$\mathbf{u}(x,y,t) := \cos(\pi t)\mathrm{Curl}\left(\sin(2\pi x)\sin(2\pi y)\right) + 128\sin(\pi t)\mathrm{Curl}\left((x-1)^2(y-1)^2x^2y^2\right),$$
$$p(x,y,t) := 128\left(x^3+y^3-1/2\right)$$

with the right-hand side $\mathbf{f} := \mathbf{u}_t - \nu\Delta\mathbf{u} + \nabla p$. Note, that $\mathbf{u}$ has zero boundary data along $\partial\Omega$ and therefore all theoretical results of this paper hold without modification.

Figure 3 shows the cumulative error $\|\nabla(\mathbf{u}-\mathbf{u}_h)\|_{\tau,h}$ for different choices of ν and different refinement levels for the classical and the modified Bernardi–Raugel finite element method with the backward Euler time stepping scheme and time step length $\tau = 10^{-4}$. One clearly sees a dependence on the parameter ν for the error of the classical method, whereas the error of the modified method is independent of ν. On mesh level 2 and $\nu = 10^{-5}$ the error of the modified Bernardi–Raugel method is about 5000 times smaller than the error of the classical method. On the opposite, the errors for $\nu = 1$ are almost identical, i.e., the error of the modified method is less than 4 percent larger than the error of the classical method. Moreover, the results of the Bernardi–Raugel finite element method do not differ qualitatively, if the Crank-Nicolson scheme is used instead of the backward Euler scheme, since the time step was chosen small enough such that the error from the space discretization dominates. To verify this, Figure 5 shows the errors for several much coarser time steps for two different refinement levels and fixed $\nu = 10^{-3}$. The main observation for the classical method is that the error is about the same even for very coarse τ, possibly because the space discretization error is huge and gives no room for improvement by better time discretization. For the modified Bernardi–Raugel method the observations are different. Here one clearly sees that the error gets smaller for smaller time steps τ up to some point where the time error is smaller than the space error.

Figure 4 shows similar results for the P_2^{bub} finite element method and Crank-Nicolson time stepping scheme with $\tau = 10^{-3}$. Here, the maximal observed improvement factor is about 200 for $\nu = 10^{-5}$ and refinement level 3, while the error of the modified method is only less than 2 percent larger compared to the classical method for $\nu = 1$. With respect to different time steps τ and other time stepping schemes similar conclusions as for the Bernardi–Raugel finite element method can be drawn, see Figure 6.

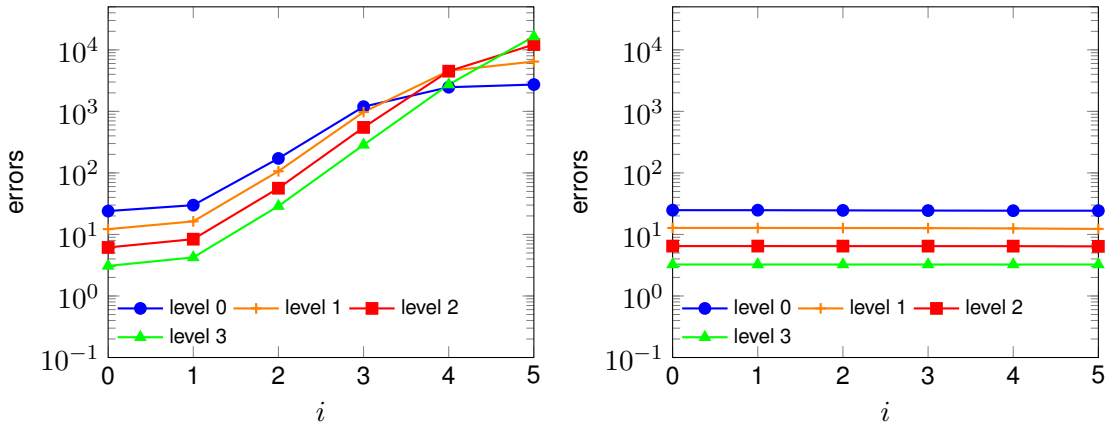

Figure 3: Example 1: Cumulative error $\|\nabla(\mathbf{u} - \mathbf{u}_h)\|_{\tau,h}$ vs the viscosity parameter $\nu = 10^{-i}$, $i = 0, \ldots, 5$, for the classical (left) and modified (right) Bernardi–Raugel finite element method with $\theta = 1$ on different refinement levels and fixed $\tau = 10^{-4}$.

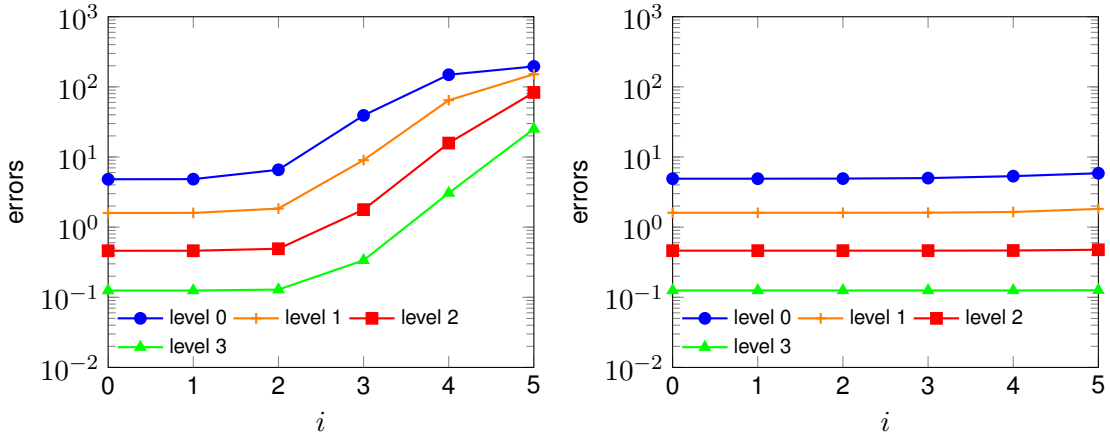

Figure 4: Example 1: Cumulative error $\|\nabla(\mathbf{u} - \mathbf{u}_h)\|_{\tau,h}$ vs the viscosity parameter $\nu = 10^{-i}$, $i = 0, \ldots, 5$, for the classical (left) and modified (right) P_2^{bub} finite element method with $\theta = 0.5$ on different refinement levels and fixed $\tau = 10^{-3}$.

6.2 Potential flow with zero right-hand side

This example studies a potential flow of the form $\mathbf{u}(t) := t\nabla h$ with the harmonic potential $h = 5x^4y + y^5 - 10x^2y^3$. This flow solves the time-dependent Stokes problem $\mathbf{u}_t - \nu\Delta u + \nabla p = 0$ with the pressure $p = -h$ [34].

Figure 7 displays the accumulated gradient error for the Crank-Nicolson scheme ($\theta = 0.5$) with fixed time step $\tau = 10^{-3}$ on different refinement levels of the initial mesh and different magnitudes of ν.

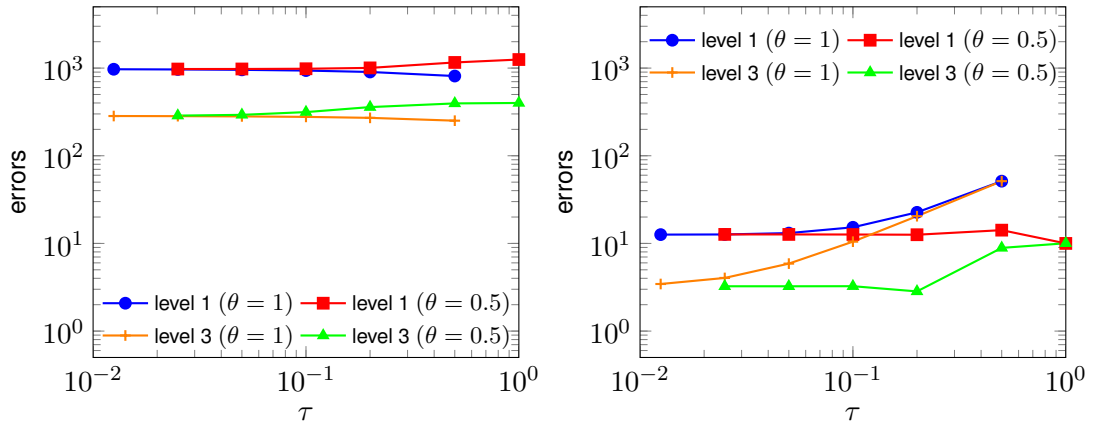

Figure 5: Example 1: Cumulative error $\|\nabla(\mathbf{u} - \mathbf{u}_h)\|_{\tau,h}$ vs the time step τ for the classical (left) and modified (right) Bernardi–Raugel finite element method on different refinement levels and fixed $\nu = 10^{-3}$.

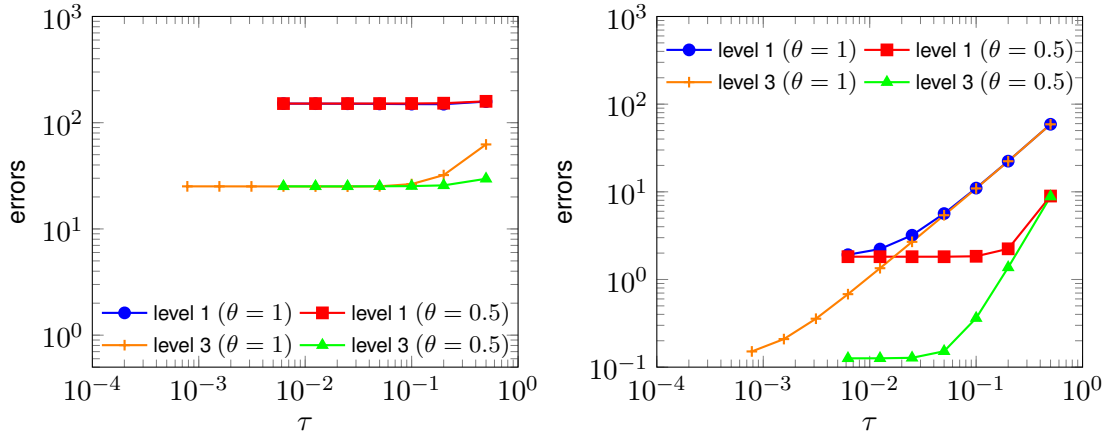

Figure 6: Example 1: Cumulative error $\|\nabla(\mathbf{u} - \mathbf{u}_h)\|_{\tau,h}$ vs the time step τ for the classical (left) and modified (right) P_2^{bub} finite element method on different refinement levels and fixed $\nu = 10^{-5}$.

While the errors are of comparable size for the larger parameters $\nu \geq 10^{-1}$, the errors of the classical method deteriorates for the smaller parameters. The errors for the modified method do not increase as dramatically as the errors of the classical method. For the finest refinement level and $\nu = 10^{-6}$ the error of the classical method is about 400 times larger than the error of the modified method. Figure 8 displays the errors for the Bernardi–Raugel finite element method with Crank-Nicolson scheme ($\theta = 1/2$) and fixed time step $\tau = 10^{-3}$. The overall observations and conclusions are very similar to the first example.

Figure 9 studies the influence of different time step sizes in both time discretization schemes on a fixed mesh. One can observe that the errors are almost identically for all different choices of τ. This makes sense, since the velocity field changes linearly in time. Even so this clearly demonstrates the influence of the reconstruction operator also in the time derivative, since this is the only difference between the both methods (the right-hand side is zero): although the time derivative $\mathbf{u}_t$ is constant, $\mathbf{u}_t$ can have a large irrotational contribution and cause errors that cannot be healed by mesh or time refinement. The pressure-robust method (or any divergence-free method) only sees the Helmholtz projector $\mathbb{P}(\mathbf{u}_T)$ of $\mathbf{u}_t$ which is zero in this example, while the classical method sees a nonzero discrete Helmholtz projector

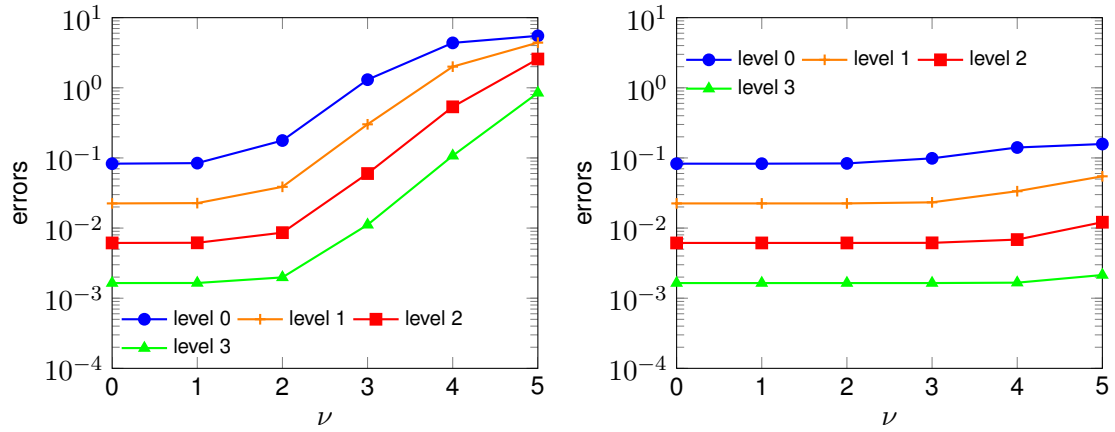

Figure 7: Example 2: Cumulative error $\|\nabla(\mathbf{u}-\mathbf{u}_h)\|_{\tau,h}$ vs the viscosity parameter $\nu = 10^{-i}$, $i = 0,\ldots,5$, for the classical (left) and modified (right) P_2^{bub} finite element method with $\theta = 0.5$ on different refinement levels and fixed $\tau = 10^{-3}$.

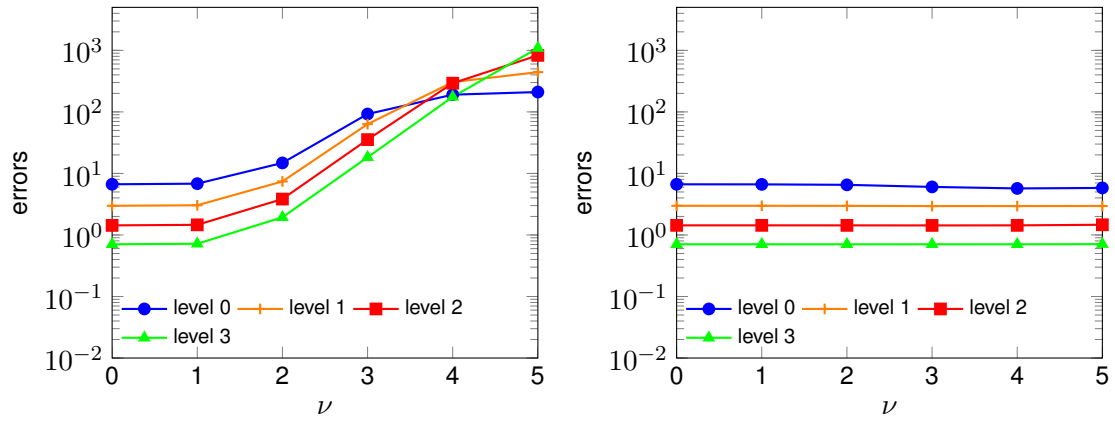

Figure 8: Example 2: Cumulative error $\|\nabla(\mathbf{u}-\mathbf{u}_h)\|_{\tau,h}$ vs the viscosity parameter $\nu = 10^{-i}$, $i = 0,\ldots,5$, for the classical (left) and modified (right) Bernardi–Raugel finite element method with $\theta = 0.5$ on different refinement levels and fixed $\tau = 10^{-3}$.

$\mathbb{P}_h(\mathbf{u}_t)$.

References

[1] Naveed Ahmed. On the grad-div stabilization for the steady Oseen and Navier–Stokes equations. *Calcolo*, pages 1–31, 2016.

[2] Naveed Ahmed, Simon Becher, and Gunar Matthies. Higher-order discontinuous Galerkin time stepping and local projection stabilization techniques for the transient Stokes problem. *Comput. Methods Appl. Mech. Engrg.*, 313:28 – 52, 2017.

[3] D. Arnold, F. Brezzi, and M. Fortin. A stable finite element for the Stokes equations. *Calcolo*, 21(4):337–344, 1984.

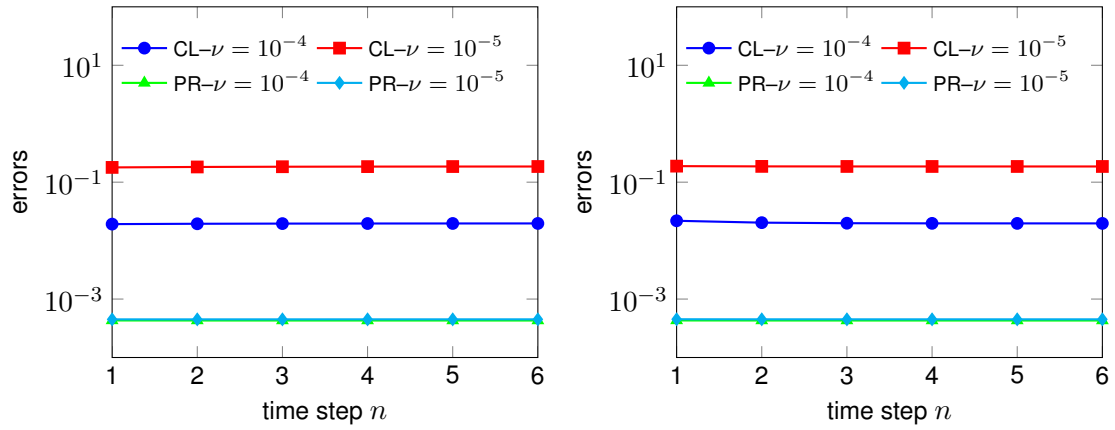

Figure 9: Example 2: Cumulative error $\|\nabla(\mathbf{u}-\mathbf{u}_h)\|_{\tau,h}$ vs the time steps $\tau = 0.1\cdot 2^{-n+1}, n = 1,\dots,6$, for the backward–Euler ($\theta = 1$, left) and Crank–Nicolson ($\theta = 0.5$, right) P_2^{bub} methods for fixed mesh with $31\ 744$ cells.

[4] D. N. Arnold and J. Qin. Quadratic velocity/linear pressure Stokes elements. In R. Vichnevetsky, D. Knight, and G. Richter, editors, *Advances in Computer Methods for Partial Differential Equations VII*, pages 28–34. IMACS, 1992.

[5] Ivo Babuska and Manil Suri. On locking and robustness in the finite element method. *SIAM J. Numer. Anal.*, 29(5):1261–1293, 1992.

[6] Gabriel R. Barrenechea and Jordi Blasco. Pressure stabilization of finite element approximations of time-dependent incompressible flow problems. *Comput. Methods Appl. Mech. Engrg.*, 197(1-4):219–231, 2007.

[7] Mine Akbas Belenli, Leo G. Rebholz, and Florentina Tone. A note on the importance of mass conservation in long-time stability of Navier-Stokes simulations using finite elements. *Appl. Math. Lett.*, 45:98–102, 2015.

[8] Pavel B. Bochev, Max D. Gunzburger, and Richard B. Lehoucq. On stabilized finite element methods for the Stokes problem in the small time step limit. *Internat. J. Numer. Methods Fluids*, 53(4):573–597, 2007.

[9] C. Brennecke, A. Linke, C. Merdon, and J. Schöberl. Optimal and pressure-independent L^2 velocity error estimates for a modified Crouzeix-Raviart Stokes element with BDM reconstructions. *J. Comput. Math.*, 33(2):191–208, 2015.

[10] F. Brezzi. New applications of mixed finite element methods. In *Proceedings of the International Congress of Mathematicians, Vol. 1, 2 (Berkeley, Calif., 1986)*, pages 1335–1347. Amer. Math. Soc., Providence, RI, 1987.

[11] F. Brezzi and M. Fortin. *Mixed and Hybrid Finite Elements*, volume 15 of *Springer Series in Computational Mathematics*. Springer, 1991.

[12] Erik Burman and Miguel A. Fernández. Galerkin finite element methods with symmetric pressure stabilization for the transient Stokes equations: stability and convergence analysis. *SIAM J. Numer. Anal.*, 47(1):409–439, 2008/09.

[13] Erik Burman and Miguel A. Fernández. Analysis of the PSPG method for the transient Stokes' problem. *Comput. Methods Appl. Mech. Engrg.*, 200(41-44):2882–2890, 2011.

[14] Jesús Carrero, Bernardo Cockburn, and Dominik Schötzau. Hybridized globally divergence-free LDG methods. I. The Stokes problem. *Math. Comp.*, 75(254):533–563 (electronic), 2006.

[15] Michael A. Case, Vincent J. Ervin, Alexander Linke, and Leo G. Rebholz. A connection between Scott-Vogelius and grad-div stabilized Taylor-Hood FE approximations of the Navier-Stokes equations. *SIAM J. Numer. Anal.*, 49(4):1461–1481, 2011.

[16] Bernardo Cockburn, Guido Kanschat, and Dominik Schötzau. A note on discontinuous Galerkin divergence-free solutions of the Navier-Stokes equations. *J. Sci. Comput.*, 31(1-2):61–73, 2007.

[17] M. Crouzeix and P.-A. Raviart. Conforming and nonconforming finite element methods for solving the stationary Stokes equations. I. *Rev. Française Automat. Informat. Recherche Opérationnelle Sér. Rouge*, 7(R-3):33–75, 1973.

[18] Daniele A. Di Pietro, Alexandre Ern, Alexander Linke, and Friedhelm Schieweck. A discontinuous skeletal method for the viscosity-dependent Stokes problem. *Comput. Methods Appl. Mech. Engrg.*, 306:175–195, 2016.

[19] John A. Evans and Thomas J. R. Hughes. Isogeometric divergence-conforming B-splines for the steady Navier-Stokes equations. *Math. Models Methods Appl. Sci.*, 23(8):1421–1478, 2013.

[20] R. Falk and M. Neilan. Stokes complexes and the construction of stable finite element methods with pointwise mass conservation. *SIAM Journal on Numerical Analysis*, 51(2):1308–1326, 2013.

[21] K. Galvin, A. Linke, L. Rebholz, and N. Wilson. Stabilizing poor mass conservation in incompressible flow problems with large irrotational forcing and application to thermal convection. *Computer Methods in Applied Mechanics and Engineering*, 237:166–176, 2012.

[22] V. Girault and P.-A. Raviart. *Finite Element Methods for Navier-Stokes Equations*, volume 5 of *Springer Series in Computational Mathematics*. Springer-Verlag, Berlin, 1986.

[23] J. Guzman and M. Neilan. Conforming and divergence-free Stokes elements in three dimensions. *IMA Journal of Numerical Analysis*, to appear, 2014.

[24] John G. Heywood and Rolf Rannacher. Finite–Element Approximation of the Nonstationary Navier–Stokes Problem. Part IV: Error analysis for second-order time discretization. *SIAM Journal on Numerical Analysis*, 27(2):353–384, 1990.

[25] Eleanor W. Jenkins, Volker John, Alexander Linke, and Leo G. Rebholz. On the parameter choice in grad-div stabilization for the Stokes equations. *Adv. Comput. Math.*, 40(2):491–516, 2014.

[26] V. John, A. Linke, C. Merdon, M. Neilan, and L. Rebholz. On the divergence constraint in mixed finite element methods for incompressible flows. *WIAS Preprint 2177*, pages 1–49, 2015. (accepted by SIAM Rev., 2016).

[27] Volker John. *Finite Element Methods for Incompressible Flow Problems*, volume 51 of *Springer Series in Computational Mathematics*. Springer International Publishing, Cham, 1st ed. edition, 2016.

[28] Volker John and Julia Novo. Analysis of the pressure stabilized Petrov-Galerkin method for the evolutionary Stokes equations avoiding time step restrictions. *SIAM J. Numer. Anal.*, 53(2):1005–1031, 2015.

[29] David Kamensky, Ming-Chen Hsu, Yue Yu, John A. Evans, Michael S. Sacks, and Thomas J.R. Hughes. Immersogeometric cardiovascular fluidâĂŞstructure interaction analysis with divergence-conforming b-splines. *Computer Methods in Applied Mechanics and Engineering*, pages –, 2016. In press.

[30] P. Lederer, A. Linke, C. Merdon, and J. Schöberl. Divergence-free reconstruction operators for pressure-robust stokes discretizations with continuous pressure finite elements. *WIAS Preprint 2288*, pages 1–23, 2016.

[31] Christoph Lehrenfeld and Joachim Schöberl. High order exactly divergence-free Hybrid Discontinuous Galerkin Methods for unsteady incompressible flows. *Comput. Methods Appl. Mech. Engrg.*, 307:339–361, 2016.

[32] A. Linke. On the role of the Helmholtz decomposition in mixed methods for incompressible flows and a new variational crime. *Comput. Methods Appl. Mech. Engrg.*, 268:782–800, 2014.

[33] A. Linke and C. Merdon. On velocity errors due to irrotational forces in the Navier-Stokes momentum balance. *Journal of Computational Physics*, 313:654–661, May 2016.

[34] A. Linke and C. Merdon. Pressure-robustness and discrete Helmholtz projectors in mixed finite element methods for the incompressible Navier–Stokes equations. *Comput. Methods Appl. Mech. Engrg.*, 311:304–326, 2016.

[35] A. Linke, C. Merdon, and W. Wollner. Optimal L^2 velocity error estimate for a modified pressure-robust crouzeix-âĂŞraviart stokes element. *IMA Journal of Numerical Analysis*, 2016.

[36] Linke, Alexander, Matthies, Gunar, and Tobiska, Lutz. Robust arbitrary order mixed finite element methods for the incompressible Stokes equations with pressure independent velocity errors. *ESAIM: M2AN*, 50(1):289–309, 2016.

[37] Gert Lube and Philipp Schroeder. Pressure-robust analysis of divergence-free and conforming fem for evolutionary incompressible Navier–Stokes flows. *arXiv.org*, pages 1–28, 2016.

[38] M. Olshanskii and A. Reusken. Grad-div stabilization for Stokes equations. *Math. Comp.*, 73(248):1699–1718, 2004.

[39] M. A. Olshanskii, G. Lube, T. Heister, and J. Löwe. Grad-div stabilization and subgrid pressure models for the incompressible Navier-Stokes equations. *Comput. Methods Appl. Mech. Engrg.*, 198(49-52):3975–3988, 2009.

[40] Vidar Thomée. *Galerkin finite element methods for parabolic problems*, volume 25 of *Springer Series in Computational Mathematics*. Springer-Verlag, Berlin, 1997.

[41] M. Vogelius. An analysis of the p-version of the finite element method for nearly incompressible materials. uniformly valid, optimal error estimates. *Numer. Math.*, 41:39–53, 1983.

[42] Shangyou Zhang. A new family of stable mixed finite elements for the 3D Stokes equations. *Math. Comp.*, 74(250):543–554, 2005.

[43] Shangyou Zhang. Divergence-free finite elements on tetrahedral grids for $k \geq 6$. *Math. Comp.*, 80(274):669–695, 2011.